Soft Computing
https://doi.org/10.1007/s00500-021-05764-8

OPTIMIZATION

Symbiotic organisms search algorithm-based security-constrained AC–DC OPF regarding uncertainty of wind, PV and PEV systems

Serhat Duman[1] · Jie Li[2] · Lei Wu[3] · Nuran Yorukeren[4]

Accepted: 19 March 2021
© The Author(s), under exclusive licence to Springer-Verlag GmbH Germany, part of Springer Nature 2021

Abstract

Nowadays, the energy obtained from different generating units in modern power systems must be suitably planned for optimal power system operating conditions. One of the methods applied for this is the optimal power flow (OPF). Thus, the optimal power flow (OPF) problem has become one of the most important power system planning and operation challenges once renewable energy sources are integrated with modern electrical power systems which have a highly nonlinear complex structure. In addition, usage of high-voltage direct current systems increases the complexity of the network in the modern power system. Using a symbiotic organisms search (SOS) algorithm, this paper focused on a solution to the security-constrained AC–DC OPF with regard to the uncertainty of wind, solar and plug-in electric vehicle (PEV) energy systems with thermal generating units. Uncertain wind speed, solar irradiance, and PEV power were modeled using Weibull, Lognormal, and Normal probability distribution functions (PDFs), respectively. Moreover, our study presents solutions to the security-constrained AC–DC OPF by involving test cases of stochastic wind, solar, and PEV energy systems on IEEE 30-bus and 57-bus test systems under various operational conditions. These can be listed as minimization of different total cost functions, improvement of voltage stability, voltage deviation and minimization of fitness function for determined N-1 contingency conditions. The SOS algorithm results were compared to the artificial bee colony, imperialist competitive, moth swarm, shuffled frog-leaping, genetic algorithm, and particle swarm optimization algorithms. These comparison results demonstrated that the SOS algorithm exhibited the capability to provide high-quality solutions to the OPF problem by satisfying both equality and inequality constraints. In addition, nonparametric Friedman and Wilcoxon tests were applied to show the statistical validity of the results obtained from the algorithms.

Keywords Modern power systems · Optimal power flow · HVDC systems · Renewable energy sources · Heuristic optimization algorithms

✉ Serhat Duman
sduman@bandirma.edu.tr

Jie Li
lijie@rowan.edu

Lei Wu
lei.wu@stevens.edu

Nuran Yorukeren
nurcan@kocaeli.edu.tr

[1] Electrical Engineering, Engineering and Natural Sciences Faculty, Bandirma Onyedi Eylul University, Bandirma 10200, Turkey

[2] Electrical and Computer Engineering, Rowan University, Glassboro, NJ 08028, USA

[3] Electrical and Computer Engineering, Stevens Institute of Technology, Hoboken, NJ 07030, USA

[4] Electrical Engineering, Engineering Faculty, Kocaeli University, Kocaeli 41380, Turkey

Published online: 27 April 2021

1 Introduction

1.1 Background, definitions and motivation

In the last decade, with the developments of technology and the rising needs of the increasing population throughout the world, the energy demands on electric power networks have increased remarkably. Nowadays, these energy demands are being met using traditional generating units operating on fossil fuels. Researchers have been investigating the use of new energy sources to replace the dependence of these traditional generating units on the limited reserves of fossil fuels with their emergent negative effects such as global warming, thinning of the ozone layer and air pollution. These new renewable energy sources (RESs) are known to be ecologically friendly and include, to name a few, wind power, photovoltaic (PV) power, hydropower, and tidal energy systems. Modern power systems have more complicated structures due to the increased penetration of RESs into electrical power networks. The difficulties in solving of the power system planning and operation problems such as economic dispatch (ED), economic and emission dispatch (EED), transmission expansion planning (TEP) and optimal power flow increase with usage of the RESs. As a result of this situation, the OPF problem incorporating RESs can be considered as one of the important problems in the planning and operation of power systems (Morshed et al. 2018; Zhao et al. 2012; Arevalo et al. 2019; Roy and Jadhav 2015; Reddy et al. 2015; Panda and Tripathy 2015).

The main purpose of the OPF problem is to minimize the total energy production cost of power system generating units by identifying optimal independent variables in the power system such as the active power and bus voltages of the generating units, transformer tap ratios and shunt capacitor values. The traditional OPF problem involves equality and inequality constraints, which include active/reactive power balance equations, generators, transformers, compensators, and system security constraints.

1.2 Literature review

In the beginning, many researchers studied the OPF problem in terms of thermal generating units and applied various heuristic methods such as the salp swarm algorithm (SSA), moth flame optimizer (MFO) algorithm, a new genetic algorithm with multi-parent crossover (GA-MPC), along with hybrid differential evolution and harmony search (Hybrid DE-HS), improved social spider optimization (ISSO) and modified global best artificial bee colony (MGABC) algorithms (El-Fergany and Hasanien 2019; Trivedi et al. 2018; Bouchekara et al. 2018; Reddy 2018; Nguyen 2019; Bansal et al. 2018). Attia et al. proposed the modified sine–cosine algorithm (MSCA) to solve the OPF problem using thermal generating units. The proposed algorithm has the ability to avoid local optima, requires less computing time in finding optimal solutions and is used to test IEEE 30-bus and IEEE 118-bus test systems under different operation conditions. Simulation results demonstrated the feasibility of MSCA as compared with SCA and other optimization algorithms (Attia et al. 2018). El-Fergany and Hasanien used the tree-seed algorithm (TSA) developed by Kiran to solve the OPF problem in large-scale electrical energy systems such as the IEEE 57-bus and IEEE 300-bus test systems (El-Fergany and Hasanien 2018). Biswas et al. attempted to solve OPF problem by using a differential evolution algorithm based on various constraint techniques in IEEE 30-bus, 57-bus and 118-bus test systems. The authors have demonstrated the superiority of the proposed approach compared to the other methods in the literature with respect to the obtained simulation results (Biswas et al. 2018a).

Recently, due to increasing global energy demands on power systems, the stress on transmission lines and buses has risen; thus, to reduce the pressure on the systems, many researchers have focused on new planning and operation studies, which incorporate adding new transmission lines or using HVDC transmission links. The advantages of HVDC transmission links which have been identified include stabilization of power systems via active power transfer through HVDC systems and reduction of power losses compared with AC transmission lines (Latorre and Ghandhari 2011; Ayan and Kılıç 2016; Kılıç et al. 2014). Babu and Palaniswami worked on the solution of an OPF with DC link placement problem using the teaching–learning-based optimization (TLBO) algorithm tested on IEEE 30-bus and IEEE 57-bus test systems (Babu and Palaniswami 2015). In another study, the same test systems were used by the authors to solve an OPF with DC link problem using the chaotic krill herd algorithm (CKHA). Simulation results of the case studies demonstrated the feasibility of the CKHA as compared with the results obtained from the TLBO algorithm (Prasad et al. 2017). Cao et al. presented a solution to the OPF problem with an AC/DC hybrid power system by using the adaptive simplified human learning optimization (ASHLO) method which was tested on IEEE 30-bus and IEEE 118-bus test systems. The ASHLO algorithm showed its superiority as compared to other well-known optimization methods (Cao et al. 2016). Kilic and Ayan focused on solving the OPF problem including a two-terminal HVDC system integrated into power systems by using a genetic algorithm (GA). The proposed GA was tested on different two-terminal systems and when the simulation results were compared to those of other methods in the literature, the authors demonstrated

the resolvability of the OPF problem using the GA method (Kılıç and Ayan 2014). In other studies, Duman applied a modified moth swarm algorithm to solve the OPF problem with a two-terminal HVDC system (Duman 2018). Sayah used a modified differential evolution method to solve the optimal reactive power dispatch (ORPD) problem for AC–DC systems (Sayah 2018); Yalcin and Arifoglu proposed to solve the ORPD problem including multi-terminal AC–DC systems using the artificial bee colony (ABC) algorithm (Yalcin and Arifoglu 2014). In addition, recently, the researchers have focused on the inclusion of voltage-source converter (VSC)-based AC/DC systems in the power flow, and they have been presented to the literature in studies where these systems are included in the solution of OPF problems (Mohammadi et al. 2020; Renedo et al. 2019; Kim et al. 2020; Abdul-hamied et al. 2020; Shaheen et al. 2020).

Nowadays, researchers are seeking to solve power system planning and operation problems in modern power systems that are using RESs. Kheshti et al. used a double-weighted particle swarm optimization algorithm to solve economic and emission problems of wind energy penetration (Kheshti et al. 2018), Chen et al. proposed a solution to hydro-thermal-wind economic dispatch problems (Chen et al. 2016) and Dubey et al. applied a hybrid flower pollination algorithm to solve the dynamic economic dispatch problem with wind power (Dubey et al. 2015). In other studies, power system planning researchers investigated short-term power system planning problems with RESs (Banerjee et al. 2016; Wang et al. 2018; Zhou et al. 2016) and in another study, they proposed a solution to the optimal reactive power dispatch problem regarding uncertainties of load, wind, and PV systems (Mohseni-Bonab et al. 2016; Liang et al. 2015; Biswas et al. 2019). In the last decades, working researchers on power system planning and operation have focused on solving the OPF problem involving RESs. Chang et al. applied the evolutionary particle swarm optimization (EPSO) algorithm to solve the OPF problem with wind generators on an IEEE 30-bus test system (Chang et al. 2014). Shi et al. used a self-adaptive evolutionary programming (SAEP) optimization algorithm to solve the OPF problem with wind-thermal generating units (Shi et al. 2012). Biswas et al. focused on solution of the OPF problem involving some well-known RESs such as wind and PV power systems. The authors successfully used the history-based parameter adaptation technique of differential evolution with superiority of feasible solutions (SHADE-SF) to solve the problem under different operational cases on an IEEE 30-bus test system (Biswas et al. 2017). The authors utilized the Gbest-guided artificial bee colony algorithm (GABC) in the solution of the OPF problem with wind power in different cases to show the applicability of the proposed algorithm (Roy and Jadhav 2015). In another study, the authors investigated the AC–DC OPF problem with wind and PEV systems using the GABC algorithm on an IEEE 30-bus test system (Jadhav and Roy 2015). Panda et al. used a modified bacteria foraging-based algorithm to solve the OPF problem with hydro-thermal-wind energy systems including STATCOM, which is one of the most important shunt flexible AC transmission systems (FACTS) devices providing reactive power in power systems (Panda et al. 2017). In addition, the solution of the OPF problem by involving configuration with different RESs was performed using two multi-objective optimization methods (Biswas et al. 2018b), the grey wolf optimizer (GWO) algorithm (Siavash et al. 2017), and the flower pollination algorithm (FPA) (Kathiravan and Kumudini Devi 2017).

In this study, we aimed to solve the security-constrained AC–DC OPF problem with wind, PV and PEV energy systems using the symbiotic organisms search (SOS) algorithm. The SOS algorithm (Cheng and Prayogo 2014) is a new optimization algorithm developed by Cheng and Prayogo, which was inspired by the symbiotic interaction behavior of organisms in an ecosystem, and it has been studied in different engineering and science fields (Ezugwu and Prayogo 2019). Recently, SOS algorithm has been used by the researchers, which are focused on to solve OPF problem in the literature. In a study, Duman proposed using SOS algorithm to solve OPF problem including valve point effects and prohibited zones under different test cases on a modified IEEE 30-bus test system. The simulation results have compared to the other results in the literature, and according to these comparative results, the SOS algorithm is much more effective to find an optimal solution than the other algorithms (Duman 2017). Prasad and Mukherjee focused on the solution OPF problem with FACTS devices, which are well known as thyristor controlled series capacitor (TCSC) and thyristor controlled phase shifter (TCPS) to test the performance of SOS algorithm on the modified IEEE 30-bus and 57-bus test systems. Authors expressed that the proposed SOS algorithm was a potential solution tool for solving OPF problem with FACTS devices according to the obtained simulation results (Prasad and Mukherjee 2016). Saha et al. aimed to solve the transient stability constrained optimal power flow problem using a novel hybrid differential evolution and symbiotic organism search algorithm (HSOS), and the proposed algorithm was tested on IEEE 30-bus and New England test systems for different test cases (Saha et al. 2020). In other studies, authors used SOS algorithm (Saha et al. 2018), and Quasi-reflection-based SOS algorithm (Saha et al. 2019a) to solve static OPF problem, and presented SOS and HSOS algorithms to the literature to solve multi-objective optimal power flow problem incorporating renewable generation unit (Saha et al. 2019b).

1.3 Contribution of the paper

According to state-of-the-art literature review, the OPF problem is one of the most important from the power system planning and operation problems. The used methods in solving of the OPF problem are divided in two section as traditional and artificial intelligence methods. The optimization algorithms are well known as artificial intelligence methods in the literature. In the beginning, the OPF problem incorporating thermal generating units was solved using optimization algorithms. The different optimization algorithms (GA, PSO, etc.) for solving the OPF problem on each study have been used to explore the success of these in finding to optimal solution of the problem, and presented to the literature. The developed optimization algorithms have attempted to find the result of problem better than previous ones on every time. Recently, FACTS devices used in OPF problem have been seen to improve voltage stability, and reduce the active, reactive power losses and fuel cost of power systems. On the other hand, the installation of HVDC transmission links in modern power system reduces the stress on power system, but the complexity of the electrical network systems increases. In addition, the usage of RES systems provides much more complexity of the power systems, and the OPF problem involving all these conditions increases the want of researchers to solve this problem.

Various variations of the OPF problem have been solved using different optimization algorithms. The SOS algorithm used in this study has been used to solve more than 700 optimization problems in the literature, and in these studies, it is seen that the algorithm converges to the optimum point quickly and its ability to avoid local traps is more successful than the optimization algorithms used. In this study, unlike the studies in the literature, the success of the SOS algorithm in solving the security-constrained OPF problem with RESs, which includes the proposed AC–DC system, was investigated considering the above-mentioned advantageous features. In addition, in the studies conducted in the literature, the use of HVDC systems, RESs and FACTS devices in OPF problems has been considered either separately or as a combination of two. This situation showed us the lack of a study examining the solution of the OPF problem using HVDC, RESs and traditional thermal generating units, given the structure of modern power systems. Moreover, considering the advantages provided by the HVDC system used in AC–DC modern power systems, these systems are included in the OPF problem involving RESs and a mathematical model of this problem is created. In the mathematical model created, wind, photovoltaic and PEV systems are considered as renewable energy sources. PEV systems are considered as energy storage sources, in short behave as load, in other words, they can be injected power to the system or can be consumed power from the system. This power behavior is modeled using the normal probability distribution function for loading and unloading behavior of plug-in electric vehicles Besides, the PEV system is only modeled the direct, under and over estimation cost models considering above situation. These cost models were modeled as different model in the reference (Arevalo et al. 2017, 2019), and in this study, the above-mentioned situations (direct, over and under estimation cost models) are modeled using the approach in references (Shi et al. (2012); Biswas et al. 2017; Biswas et al. 2018b) and presented to the literature.

In the literature, the transmission line capacities and load bus voltage limits are widely considered as security constraints in the solution of the traditional OPF problem and the OPF problem with RESs. Our study, presented differently from the literature in this paper, has taken into account these security constraints simultaneously with the generator units' generating constraints, and prohibited operating zones (POZs). In addition, the dependent and independent variables of a two-terminal HVDC system were integrated with the OPF problem with RESs and the most favorable probability density functions, which are Weibull, Lognormal and Normal, were selected to compose a stochastic model of the RESs used. The simulation results of the SOS approach were compared with the artificial bee colony (ABC) algorithm (Karaboga and Basturk 2007), imperialist competitive algorithm (ICA) (Atashpaz-Gargari and Lucas 2007), moth swarm algorithm (MSA) (Mohamed et al. 2017), shuffled frog-leaping algorithm (SFLA) (Eusuff et al. 2006), genetic algorithm (GA) (Goldberg 1989), and particle swarm optimization (PSO) (Kennedy and Eberhart 1995). The contributions of this paper can be listed as below:

- The OPF problem incorporating stochastic wind power, photovoltaic system, PEV system, and different objective functions, which are with valve point effect, prohibited zones, and emission and carbon tax has not been reported so far.
- The proposed security-constrained OPF problem with RESs incorporating AC–DC system was used by the authors and has not been reported so far; therefore, a formulation of this proposed problem is represented in this paper.
- In this study, the combination of the PV and PEV power systems was considered as a generating unit. Cost models for overestimation and underestimation situations of the combination model were studied in this paper.
- To show resolvability and feasibility of the proposed AC–DC OPF problem with RESs, the SOS, ABC, ICA,

MSA, SFLA, GA, and PSO optimization algorithms were applied under the different cases to IEEE 30-bus and 57 bus test systems.

- According to the simulation results, Wilcoxon pairwise comparison was used to show the superiority of the SOS algorithm used in the solution of the problem compared to other algorithms, and the Friedman test was used for multiple comparisons between algorithms used more than two.

1.4 Organization of the paper

The organization of the paper is summarized as follows. The formulation of the AC–DC OPF problem with wind, PV and PEV energy systems is presented in Sect. 2. Section 3 presents the RES uncertainty and power models. The SOS optimization algorithm is described in Sects. 4, and 5 explains the simulation studies for different operating cases. Section 6 presents the conclusions regarding the proposed OPF problem.

2 Formulation of AC–DC optimal power flow with RESs

The OPF problem is identified as one of the modern electrical system planning problems. In this study, the AC–DC OPF problem was investigated with wind, PV, and PEV systems. The main goal of the AC–DC OPF problem was to minimize an identified objective function by finding the optimum independent variables within the system equality and inequality constraints.

2.1 Traditional OPF problem

The formulation of the traditional OPF problem can be mathematically explained as follows:

$$\text{Minimize } f_{\text{obj}}(\boldsymbol{A},\boldsymbol{B}) \tag{1}$$

$$\text{Subject to } \begin{cases} g(\boldsymbol{A},\boldsymbol{B}) = 0 \\ h(\boldsymbol{A},\boldsymbol{B}) \le 0 \end{cases} \tag{2}$$

where $f_{\text{obj}}(\boldsymbol{A},\boldsymbol{B})$ is the objective function, $\boldsymbol{A}$ and $\boldsymbol{B}$ are the dependent and the independent variables, and $g(\boldsymbol{A},\boldsymbol{B})$ and $h(\boldsymbol{A},\boldsymbol{B})$ are the equality and the inequality constraints, respectively.

2.2 Security-constrained OPF problem

The formulation of the security-constrained OPF problem can be described as follows:

$$\text{Minimize } f_{\text{obj}}(\boldsymbol{A_0},\boldsymbol{B_0}) \tag{3}$$

$$\text{Subject to } \begin{cases} g_a(\boldsymbol{A_a},\boldsymbol{B_0}) = 0 & \boldsymbol{a} = 0,1,\ldots,\boldsymbol{c} \\ h_a(\boldsymbol{A_a},\boldsymbol{B_0}) \le 0 & \boldsymbol{a} = 0,1,\ldots,\boldsymbol{c} \end{cases} \tag{4}$$

where $\boldsymbol{A_0}$ and $\boldsymbol{B_0}$ are indicated as the dependent and the independent variables under pre-contingency cases, $\boldsymbol{A_a}$ is the dependent variables of the ath contingency case, $\boldsymbol{c}$ is the number of contingency cases.

2.3 Dependent variables

The dependent variables of the proposed OPF problem are defined as follows:

$$\begin{aligned} \boldsymbol{A} &= [\boldsymbol{A_{AC}},\boldsymbol{A_{DC}}] \\ \boldsymbol{A_{AC}} &= [P_{\text{THG}_1}, V_{L_1}\ldots V_{L_{\text{NPQ}}}, Q_{\text{THG}_1}\ldots Q_{\text{THG}_{\text{NTHG}}}, \\ &\quad Q_{\text{WS}_1}\ldots Q_{\text{WS}_{\text{NW}}}, Q_{\text{PVS}_1}\ldots Q_{\text{PVS}_{\text{NPV}}}, Q_{\text{PPEV}_1}\ldots Q_{\text{PPEV}_{\text{NPPEV}}}, S_{l_1}\ldots S_{l_{\text{NTL}}}] \\ \boldsymbol{A_{DC}} &= [t_r, t_i, \alpha, \gamma, v_{dr}, v_{di}] \end{aligned} \tag{5}$$

where P_{THG1} is the active power of the slack generator, V_L is voltage magnitudes of the load (PQ) buses, Q_{THG}, Q_{WS}, Q_{PVS}, and Q_{PPEV} are the reactive power of thermal generators, wind power, PV, and combined PV and PEV systems, and S_L is apparent power of transmission lines. NPQ and NTL are numbers of PQ buses and transmission lines. Transformer tap ratio values of rectifier and inverter sides are depicted as t_r and t_i, α and γ are, respectively, the ignition delay and extinction advance angles. v_{dr} and v_{di} are DC voltage values of the rectifier and inverter terminals.

2.4 Independent variables

The independent variables of the proposed OPF problem can be described as follows:

$$\begin{aligned} \boldsymbol{B} &= [\boldsymbol{B_{AC}},\boldsymbol{B_{DC}}] \\ \boldsymbol{B_{AC}} &= [P_{\text{THG}_2}\ldots P_{\text{THG}_{\text{NTHG}}}, P_{\text{WS}_1}\ldots P_{\text{WS}_{\text{NW}}}, P_{\text{PVS}_1}\ldots P_{\text{PVS}_{\text{NPV}}}, \\ &\quad P_{\text{PPEVS}_1}\ldots P_{\text{PPEVS}_{\text{NPPEV}}}, V_{G_1}\ldots V_{G_{\text{NG}}}, T_1\ldots T_{\text{NT}}, Q_{S_1}\ldots Q_{S_{\text{NC}}}] \\ \boldsymbol{B_{DC}} &= [P_r, P_i, Q_r, Q_i, i_d] \end{aligned} \tag{6}$$

where P_{THG} is the active power of thermal generators except for the swing generator, P_{WS} is the active power of wind farm, P_{PVS} is the active power of the PV system, P_{PPEVS} P_{PPEVS} is the active power of the combined PV and PEV systems, V_G is the voltage values of all generator buses including thermal generators, wind farm, PV, and combined PV and PEV systems. Q_S and T are, respectively, the shunt VAR compensation and the tap settings of transformers. NTHG, NW, NPV, NPPEV, NG, NT, and NC are numbers of thermal generation units, wind farms, PV units, combined systems, and generator buses (including thermal, wind, PV and combined units), tap regulating

transformers, and compensators. P_r, P_i, Q_r and Q_i are the active and reactive power values of the rectifier and inverter sides, and i_d is the direct current.

2.5 Modeling of DC transmission link

In this study, the DC transmission link was based on the widely accepted assumptions in the literature. These assumptions are explained in detail in Refs. (Kılıç et al. (2014); Kılıç and Ayan 2014). A two-terminal HVDC transmission system is shown in Fig. 1 (Ayan and Kılıç 2016; Kılıç et al. 2014; Kılıç and Ayan 2014), in which v_r, v_i, i_r, and i_i are, respectively, the ac voltage values (rms), and the currents at the AC sides of the rectifier and inverter. δ_r, δ_i, ξ_r, and ξ_i are the phase angles, and AC current angles, r_{dc} is the DC link resistance.

The equations of the rectifier terminal can be explained for a two-terminal HVDC system as follows (Ayan and Kılıç 2016; Kılıç et al. 2014; Kılıç and Ayan 2014):

$$\begin{aligned} v_{dor} &= kt_r v_r \quad \Rightarrow k = \frac{3\sqrt{2}}{\pi} \\ v_{dr} &= v_{dor}\cos\alpha - r_{cr} i_d \quad \Rightarrow r_{cr} = \frac{3x_{cr}}{\pi} \\ P_r &= v_{dr} i_d \\ \varphi_r &= \cos^{-1}\left(v_{dr}/v_{dor}\right) \\ Q_r &= |P_r \tan\phi_r| \end{aligned} \tag{7}$$

where v_{dor}, r_{cr} and φ_r are, respectively, the open circuit DC voltage value, the commutating resistance, and the phase angle at the rectifier side. The inverter terminal equations are given in (8) (Ayan and Kılıç (2016); Kılıç et al. 2014; Kılıç and Ayan 2014):

$$\begin{aligned} v_{doi} &= kt_i v_i \quad \Rightarrow k = \frac{3\sqrt{2}}{\pi} \\ v_{di} &= v_{doi}\cos\gamma - r_{ci} i_d \quad \Rightarrow r_{ci} = \frac{3x_{ci}}{\pi} \\ P_i &= v_{di} i_d \\ \varphi_i &= \cos^{-1}\left(v_{di}/v_{doi}\right) \\ Q_i &= |P_i \tan\phi_i| \end{aligned} \tag{8}$$

where v_{doi}, r_{ci} and φ_i are, respectively, the open circuit DC voltage value, the commutating resistance, and the phase angle at the inverter side. The equivalent circuit of a two-terminal HVDC link system is shown in Fig. 2 (Ayan and Kılıç 2016; Kılıç et al. 2014; Kılıç and Ayan 2014). The voltage balance of the DC system is shown in (9).

$$v_{dr} - v_{di} - r_{dc} i_d = 0 \tag{9}$$

2.6 Fuel cost model of thermal generators

The classical fuel cost function in the thermal generating units is defined as a quadratic cost function in (10), or as a quadratic function with valve-point effects in (11). In the valve-point effect model, the different ejector groups in the valves control the steam input to the turbine. The fuel cost value of the system will rise with the opening–closing process of the valves. In order to accurately model the fuel cost of the process, sinusoidal terms and coefficients describing the valve-point loading effect must be added to the traditional fuel cost function (Biswas et al. 2017; 2018a, b), where x_i, y_i, and z_i are fuel cost coefficients of the ith thermal generator, and d_i and e_i are the valve-point loading effect coefficients.

$$\mathrm{CF}_1(P_{\mathrm{THG}}) = \sum_{i=1}^{\mathrm{NTHG}} x_i + y_i P_{\mathrm{THG}_i} + z_i P_{\mathrm{THG}_i}^2 \tag{10}$$

$$\mathrm{CF}_2(P_{\mathrm{THG}}) = \mathrm{CF}_1(P_{\mathrm{THG}}) + \sum_{i=1}^{\mathrm{NTHG}} \left| d_i \sin\left(e_i\left(P_{\mathrm{THG}_i}^{\min} - P_{\mathrm{THG}_i}\right)\right)\right| \tag{11}$$

2.7 Prohibited operating zones

A thermal generator with POZs can be defined as follows (Duman 2017).

$$\begin{aligned} & P_{\mathrm{THG}i,\,\min} \le P_{\mathrm{THG}i} \le P^L_{\mathrm{THG}i,\,1} \\ & P^U_{\mathrm{THG}i,\,h-1} \le P_{\mathrm{THG}i} \le P^L_{\mathrm{THG}i,\,h} \quad h = 2, 3, \ldots, ri \\ & P^U_{\mathrm{THG}i,\,ri} \le P_{\mathrm{THG}i} \le P^L_{\mathrm{THG}i,\,\max} \end{aligned} \tag{12}$$

where ri is the total number of the POZs, h is the number of the POZs, $P^U{}_{\mathrm{THG}i,\,h-1}$ and $P^L{}_{\mathrm{THG}i,\,h}$ is the upper and lower limits of the $(h-1)$th POZ of the ith generator. The characteristics of the fuel cost with and without valve point

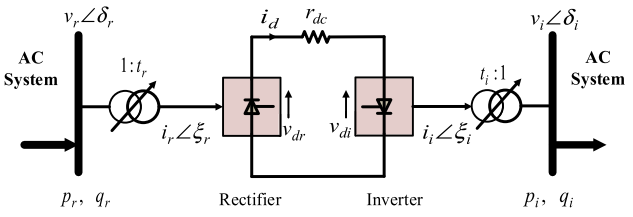


Fig. 1 Two terminal HVDC transmission system

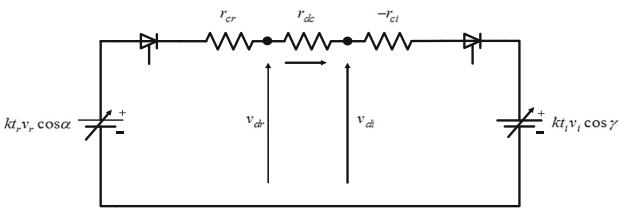


Fig. 2 The equivalent circuit of a HVDC link system

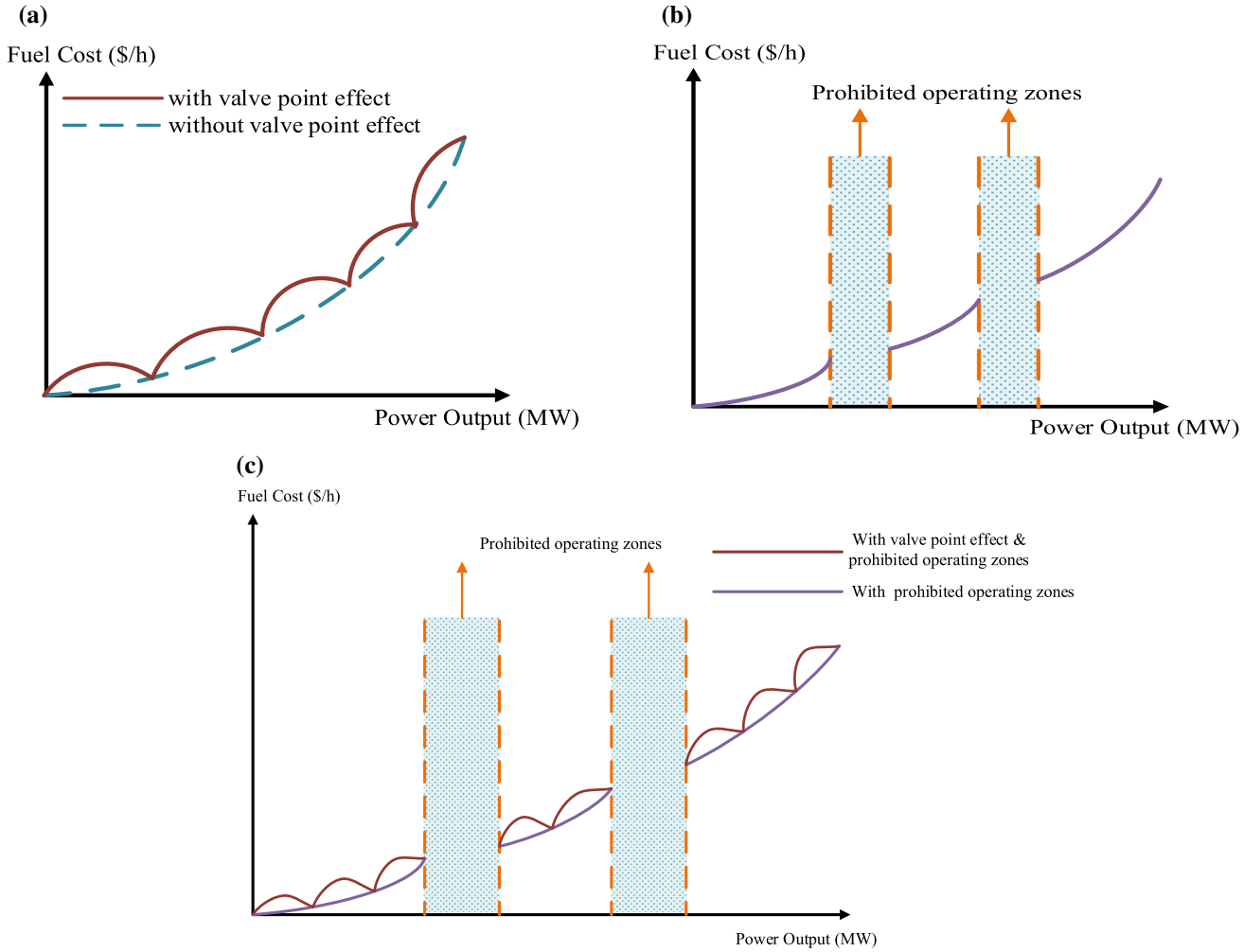


Fig. 3 Fuel cost curves, (**a**) with and without valve-point effect, (**b**) with prohibited operating zones, (**c**) with valve-point effect and prohibited operating zones

effect, and POZs of the thermal generating units are shown in Fig. 3 (Naderi et al. 2019, 2021).

2.8 Emission and carbon tax model

The total emission from a traditional generating unit with fossil fuel can be mathematically described as in (13) (Biswas et al. 2017; 2018a), where σ_i, β_i, τ_i, ω_i, and μ_i are emission coefficients of the ith thermal generating unit. In recent years, due to increasing global warming, a carbon tax for air pollution has been added to the total emission value, as shown in (14), where C_E and C_{tax} can be identified as emission cost and tax, respectively.

$$F_E = \sum_{i=1}^{\mathrm{NTHG}} \left[\left(\sigma_i + \beta_i P_{\mathrm{THG}_i} + \tau_i P_{\mathrm{THG}_i}^2 \right) \times 0.01 + \omega_i \exp(\mu_i \times P_{\mathrm{THG}_i}) \right] \tag{13}$$

$$C_E = C_{\mathrm{tax}} \times F_E \tag{14}$$

2.9 Direct cost models of wind, PV and PEV systems

Renewable energy sources do not need any fossil fuel sources. In the case that these RESs are had the by independent system operator (ISO), this operator has to pay a price depending on the scheduled power of the RESs. The cost model of a wind power source can be defined via a linear function of scheduled wind power (Biswas et al. 2017, 2018b), where ww, i, and $P_{\mathrm{WS},\ i}$ are the cost coefficient and scheduled power of the ith wind farm.

$$\mathrm{CF}_{w,i}\left(P_{\mathrm{WS},i}\right) = \mathrm{ww},\ i \times P_{\mathrm{WS},i} \tag{15}$$

The cost model of a PV power source is identified as a linear function of scheduled PV power (Biswas et al. 2017, 2018b), where pv, i, and $P_{\mathrm{PVS},\ i}$ are the cost coefficient and scheduled power of the ith PV power unit.

$$\mathrm{CF}_{\mathrm{pv},i}\left(P_{\mathrm{PVS},i}\right) = \mathrm{pv},\ i \times P_{\mathrm{PVS},i} \tag{16}$$

In this study, a combination of the ith PV system and the PEV system can be mathematically explained as follows.

$$CF_{\mathrm{ppev},i}\left(P_{\mathrm{PPEVS},i}\right) = \left(\mathrm{pv},\ i \times P_{\mathrm{PVS},i}\right) + \left(\mathrm{pev},\ i \times P_{\mathrm{PEVS},i}\right) \tag{17}$$

where pev, i and $P_{\mathrm{PEVS},\ i}$ are the cost coefficient and scheduled power of the ith PEV unit.

2.10 Uncertain cost models of wind, PV and PEV systems

In this study, the uncertain cost models of wind, PV, and a combination model of PV and PEV systems were constituted by considering overestimation and underestimation situations. Cost models for these situations for wind power are mathematically described as follows (Biswas et al. 2017, 2018b).

$$\begin{aligned}\mathrm{CF}_{\mathrm{Ow},i}\left(P_{\mathrm{WS},i} - P_{\mathrm{wav},i}\right) &= C_{\mathrm{Ow},i}\left(P_{\mathrm{WS},i} - P_{\mathrm{wav},i}\right)\\ &= C_{\mathrm{Ow},i}\int_{0}^{P_{\mathrm{WS},i}}\left(P_{\mathrm{WS},i} - p_{w,i}\right)f_w\left(p_{w,i}\right)\mathrm{dp}_{w,i}\end{aligned} \tag{18}$$

$$\begin{aligned}\mathrm{CF}_{\mathrm{Uw},i}\left(P_{\mathrm{wav},i} - P_{\mathrm{WS},i}\right) &= C_{\mathrm{Uw},i}\left(P_{\mathrm{wav},i} - P_{\mathrm{WS},i}\right)\\ &= C_{\mathrm{Uw},i}\int_{P_{\mathrm{WS},i}}^{P_{\mathrm{wr},i}}\left(p_{w,i} - P_{\mathrm{WS},i}\right)f_w\left(p_{w,i}\right)\mathrm{dp}_{w,i}\end{aligned} \tag{19}$$

where $\mathrm{CF}_{\mathrm{Ow},\ i}$ and $\mathrm{CF}_{\mathrm{Uw},\ i}$ are the uncertainty cost values for overestimation and underestimation of a wind farm, $C_{\mathrm{Ow},\ i}$ and $C_{\mathrm{Uw},\ i}$ are the uncertainty cost coefficients, and $P_{\mathrm{wav},\ i}$, $P_{\mathrm{wr},\ i}$ are, respectively, the available power and rated power of the ith wind farm.

The cost model for the uncertain situations of the PV power system from the RESs was considered the same as for the wind power. The overestimation and underestimation were modeled using the approach in Refs (Shi et al. (2012); Biswas et al. 2017; Biswas et al. 2018b). Cost models for overestimation and underestimation PV system situations are mathematically described as follows.

$$\begin{aligned}\mathrm{CF}_{\mathrm{Opv},i}\left(P_{\mathrm{PVS},i} - P_{\mathrm{PVav},i}\right) &= C_{\mathrm{Opv},i}\left(P_{\mathrm{PVS},i} - P_{\mathrm{PVav},i}\right)\\ &= C_{\mathrm{Opv},i} * f_{\mathrm{PV}}\left(P_{\mathrm{PVav},i} < P_{\mathrm{PVS},i}\right)\\ &\quad * \left[P_{\mathrm{PVS},i} - E\left(P_{\mathrm{PVav},i} < P_{\mathrm{PVS},i}\right)\right]\end{aligned} \tag{20}$$

$$\begin{aligned}CF_{\mathrm{Upv},i}\left(P_{\mathrm{PVav},i} - P_{\mathrm{PVS},i}\right) &= C_{\mathrm{Upv},i}\left(P_{\mathrm{PVav},i} - P_{\mathrm{PVS},i}\right)\\ &= C_{\mathrm{Upv},i} * f_{\mathrm{PV}}\left(P_{\mathrm{PVav},i} > P_{\mathrm{PVS},i}\right)\\ &\quad * \left[E\left(P_{\mathrm{PVav},i} > P_{\mathrm{PVS},i}\right) - P_{\mathrm{PVS},i}\right]\end{aligned} \tag{21}$$

where $\mathrm{CF}_{\mathrm{Opv},\ i}$ and $\mathrm{CF}_{\mathrm{Upv},\ i}$ are the uncertainty cost values for overestimation and underestimation of the ith PV power system, $C_{\mathrm{Opv},\ i}$ and $C_{\mathrm{Upv},\ i}$ are the uncertainty cost coefficients, and $P_{\mathrm{PVav},\ i}$ is the available power of the ith PV power system.

In our study, the combination of the PV and PEV power systems was considered as a generating unit. Cost models for overestimation and underestimation situations of the combination model were defined by the modeling approach in Refs. (Shi et al. (2012); Biswas et al. 2017; Biswas et al. 2018b).

$$\begin{aligned}&\mathrm{CF}_{\mathrm{Oppev},i}\left(P_{\mathrm{PPEVS},i} - P_{\mathrm{PPEVav},i}\right)\\ &\quad = C_{\mathrm{Oppev},i}\left(P_{\mathrm{PPEVS},i} - P_{\mathrm{PPEVav},i}\right)\\ &\quad = C_{\mathrm{Oppev},i} * f_{\mathrm{PPEV}}\left(P_{\mathrm{PPEVav},i} < P_{\mathrm{PPEVS},i}\right) *\\ &\qquad \left[P_{\mathrm{PPEVS},i} - E\left(P_{\mathrm{PPEVav},i} < P_{\mathrm{PPEVS},i}\right)\right]\end{aligned} \tag{22}$$

$$\begin{aligned}&\mathrm{CF}_{\mathrm{Uppev},i}\left(P_{\mathrm{PPEVav},i} - P_{\mathrm{PPEVS},i}\right)\\ &\quad = C_{\mathrm{Uppev},i}\left(P_{\mathrm{PPEVav},i} - P_{\mathrm{PPEVS},i}\right)\\ &\quad = C_{\mathrm{Uppev},i} * f_{\mathrm{PPEV}}\left(P_{\mathrm{PPEVav},i} > P_{\mathrm{PPEVS},i}\right) *\\ &\qquad \left[E\left(P_{\mathrm{PPEVav},i} > P_{\mathrm{PPEVS},i}\right) - P_{\mathrm{PPEVS},i}\right]\end{aligned} \tag{23}$$

where $\mathrm{CF}_{\mathrm{Oppev},\ i}$ and $\mathrm{CF}_{\mathrm{Uppev},\ i}$ are the uncertainty cost values for overestimation and underestimation of the ith combination system, $C_{\mathrm{Oppev},\ i}$ and $C_{\mathrm{Uppev},\ i}$ are the uncertainty cost coefficients, and $P_{PPEVav,i}$ is the available power of the ith combination system.

2.11 Objective functions

The objective function of the proposed AC–DC OPF problem with wind, PV and PEV electric energy sources for different cases can be defined as follows:

2.11.1 Total cost model

The total cost model of the proposed OPF problem is identified as objective function in (24).

$$
\begin{aligned}
f_{\text{obj}}(A,B) = F_{\text{obj}_1} &= \text{CF}_1(P_{\text{THG}}) \\
&+ \sum_{i=1}^{\text{NW}} \left(\text{CF}_{w,i}\left(P_{\text{WS},i}\right) + \text{CF}_{\text{Ow},i}\left(P_{\text{WS},i} - P_{\text{wav},i}\right) + \text{CF}_{\text{Uw},i}\left(P_{\text{wav},i} - P_{\text{WS},i}\right)\right) \\
&+ \sum_{i=1}^{\text{NPV}} \left(\text{CF}_{\text{pv},i}\left(P_{\text{PVS},i}\right) + \text{CF}_{\text{Opv},i}\left(P_{\text{PVS},i} - P_{\text{PVav},i}\right) + \text{CF}_{\text{Upv},i}\left(P_{\text{PVav},i} - P_{\text{PVS},i}\right)\right) \\
&+ \sum_{i=1}^{\text{NPPEV}} \left(\text{CF}_{\text{ppev},i}\left(P_{\text{PPEVS},i}\right) + \text{CF}_{\text{Oppev},i}\left(P_{\text{PPEVS},i} - P_{\text{PPEVav},i}\right) + \text{CF}_{\text{Uppev},i}\left(P_{\text{PPEVav},i} - P_{\text{PPEVS},i}\right)\right)
\end{aligned} \tag{24}
$$

2.11.2 Total cost model with valve point effect

The objective function of the proposed OPF problem is defined as follows in (25).

$$
\begin{aligned}
f_{\text{obj}}(A,B) = F_{\text{obj}_2} &= \sum_{i=1}^{\text{NTHG}} \left(x_i + y_i P_{\text{THG}_i} + z_i P_{\text{THG}_i}^2\right) + \left|d_i \times \sin\left(e_i \times \left(P_{\text{THG}_i}^{\min} - P_{\text{THG}_i}\right)\right)\right| \\
&+ \sum_{i=1}^{\text{NW}} \left(\text{CF}_{w,i}\left(P_{\text{WS},i}\right) + \text{CF}_{\text{Ow},i}\left(P_{\text{WS},i} - P_{\text{wav},i}\right) + \text{CF}_{\text{Uw},i}\left(P_{\text{wav},i} - P_{WS,i}\right)\right) \\
&+ \sum_{i=1}^{\text{NPV}} \left(\text{CF}_{\text{pv},i}\left(P_{\text{PVS},i}\right) + \text{CF}_{\text{Opv},i}\left(P_{\text{PVS},i} - P_{\text{PVav},i}\right) + \text{CF}_{Upv,i}\left(P_{\text{PVav},i} - P_{\text{PVS},i}\right)\right) \\
&+ \sum_{i=1}^{\text{NPPEV}} \left(\text{CF}_{\text{ppev},i}\left(P_{\text{PPEVS},i}\right) + \text{CF}_{\text{Oppev},i}\left(P_{\text{PPEVS},i} - P_{\text{PPEVav},i}\right) + \text{CF}_{\text{Uppev},i}\left(P_{\text{PPEVav},i} - P_{\text{PPEVS},i}\right)\right)
\end{aligned} \tag{25}
$$

2.11.3 Total cost model with emission and tax

The objective function of the proposed OPF problem is given as in (26).

$$
f_{\text{obj}}(A,B) = F_{\text{obj}_4} = F_{\text{obj}_1} + C_E \tag{26}
$$

2.11.4 Enhancement of the voltage stability of the power systems

Increasing energy demands raise the stress on transmission lines, thus revealing the stability problems in the power systems. Voltage stability is one of the important stability problems in power systems and may be seen in particular as a result of an increase in load at the PQ bus, a change in the power system configuration, or a disturbance in the power grids. The *L*-index values of PQ buses are a good indicator of the voltage stability in a modern power system. The *L*-index value is expected to be between 0 and 1, while a lower *L*-index value for a modern power grid indicates a more stable status (Duman 2018; Chaib et al. 2016).

$$
L_j = \left|1 - \sum_{i=1}^{\text{NG}} F_{ji} \frac{V_i}{V_j}\right| \quad \text{where } j = 1, 2, ..., \text{NPQ} \tag{27}
$$

$$
F_{ji} = -[\mathbf{Y_{LL}}]^{-1}[\mathbf{Y_{LG}}] \tag{28}
$$

The NG is number of generator buses that are equipped with thermal, wind, PV or PEV generating units. NPQ is number of the PQ buses. The *L*-index value of the *j*th bus is defined as L_j. $\mathbf{Y_{LL}}$ and $\mathbf{Y_{LG}}$ are calculated from the system YBUS matrix after separating the PQ buses and all generating unit buses, as shown in (29).

$$
\begin{bmatrix} I_L \\ I_G \end{bmatrix} = [\boldsymbol{Y_{bus}}] \begin{bmatrix} V_L \\ V_G \end{bmatrix} = \begin{bmatrix} Y_{\text{LL}} & Y_{\text{LG}} \\ Y_{\text{GL}} & Y_{\text{GG}} \end{bmatrix} \begin{bmatrix} V_L \\ V_G \end{bmatrix} \tag{29}
$$

The maximum value of the *L*-indices is identified as the objective function, shown as below:

$$
f_{\text{obj}}(A,B) = F_{\text{obj}_5} = \min(L_{\max}) = \min\left(\max\left(L_j\right)\right) \tag{30}
$$

2.11.5 Voltage deviation

The value of voltage deviation in modern power grids can be calculated as follows.

$$f_{\text{obj}}(A,B) = F_{\text{obj}_6} = \text{VD} = \left(\sum_{i=1}^{\text{NPQ}} |V_{L_i} - 1|\right) \tag{31}$$

2.12 Equality constraints

Equality constraints in AC–DC OPF problem include the power balance equations in the power grid. These equations are shown in (32)-(33).

$$\begin{aligned} &P_{\text{Gk}} - P_{\text{Lk}} - P_{\text{Dk}} \\ &\quad - V_k \sum_{m=1}^{N_{\text{bus}}} V_m [G_{\text{km}} \cos(\delta_{\text{km}}) + B_{\text{km}} \sin(\delta_{\text{km}})] \\ &\quad = 0 \quad \forall k \in N_{\text{bus}} \end{aligned} \tag{32}$$

$$\begin{aligned} &Q_{Gk} + Q_{Sk} - Q_{Lk} - Q_{Dk} \\ &\quad - V_k \sum_{m=1}^{N_{bus}} V_m [G_{km} \sin(\delta_{km}) - B_{km} \cos(\delta_{km})] = 0 \ \forall k \in N_{bus} \end{aligned} \tag{33}$$

where P_{Gk}, P_{Lk}, and P_{Dk} are, respectively, active powers of the kth generating unit (including thermal, wind, PV, and combined units), the load bus, and the DC link. The Q_{Gk}, Q_{Sk}, Q_{Lk}, and Q_{Dk} are, respectively, reactive powers of the kth generating unit (including thermal, wind, PV, and PEV units), the shunt VAR compensator, the load bus, and the DC link in the power grid. The N_{bus} is number of buses, V_k, and V_m are the voltage magnitudes at buses k and m, δ_{km} is the angle difference of voltage phasor values at buses k and m, and G_{km} and B_{km} are the conductance and susceptance of the transmission line between buses k and m. The structure of the power grid is shown in Fig. 4 (Ayan and Kılıç 2016; Kılıç et al. 2014; Kılıç and Ayan 2014).

The active and reactive power equations of the rectifier and inverter connected to buses in the power system are mathematically defined as follows:

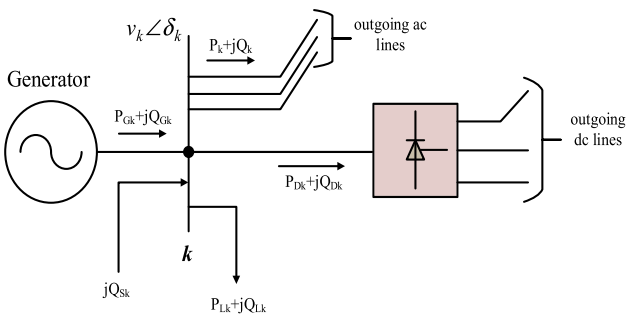


Fig. 4 AC bus connected to DC link

$$\begin{aligned} P_{\text{Dk}} &= P_r \\ Q_{\text{Dk}} &= Q_r \\ P_{\text{Dk}} &= -P_i \\ Q_{\text{Dk}} &= Q_i \end{aligned} \tag{34}$$

where P_r, and Q_r are, respectively, active and reactive power at the rectifier side, P_i, and Q_i are, respectively, active and reactive power at the inverter side.

2.13 Inequality constraints

2.13.1 Generator constraints

Lower and upper limits on active and reactive power outputs of thermal, wind, PV and PEV generation units, as well as voltage magnitudes of generating units (including thermal, wind, PV and PEV units) are identified as in (35).

$$\begin{aligned} P_{\text{THG}_i,\min} \le P_{\text{THG}_i} \le P_{\text{THG}_i,\max} \quad &\forall i \in \text{NTHG} \\ P_{\text{WS}_i,\min} \le P_{\text{WS}_i} \le P_{\text{WS}_i,\max} \quad &\forall i \in \text{NW} \\ P_{\text{PVS}_i,\min} \le P_{\text{PVS}_i} \le P_{\text{PVS}_i,\max} \quad &\forall i \in \text{NPV} \\ P_{\text{PPEVS}_i,\min} \le P_{\text{PPEVS}_i} \le P_{\text{PPEVS}_i,\max} \quad &\forall i \in \text{NPPEV} \\ Q_{\text{THG}_i,\min} \le Q_{\text{THG}_i} \le Q_{\text{THG}_i,\max} \quad &\forall i \in \text{NTHG} \\ Q_{\text{WS}_i,\min} \le Q_{\text{WS}_i} \le Q_{\text{WS}_i,\max} \quad &\forall i \in \text{NW} \\ Q_{\text{PVS}_i,\min} \le Q_{\text{PVS}_i} \le Q_{\text{PVS}_i,\max} \quad &\forall i \in \text{NPV} \\ Q_{\text{PPEVS}_i,\min} \le Q_{\text{PPEVS}_i} \le Q_{\text{PPEVS}_i,\max} \quad &\forall i \in \text{NPPEV} \\ V_{G_i,\min} \le V_{G_i} \le V_{G_i,\max} \quad &\forall i \in \text{NG} \end{aligned} \tag{35}$$

2.13.2 Transformer constraints

Minimum and maximum limits of the transformer tap ratio at the ith bus are shown in (36).

$$T_{i,\min} \le T_i \le T_{i,\max} \quad \forall i \in \text{NT} \tag{36}$$

where $T_{i.\ \min}$ and $T_{i,\ \max}$ are minimum and maximum tap ratio values of the transformers.

2.13.3 Compensators constraints

Feasible operating ranges of the shunt VAR compensators are shown in (37), where $Q_{\text{Si, min}}$ and $Q_{\text{Si, max}}$ are lower and upper limits of the shunt VAR compensators.

$$Q_{\text{Si},\min} \le Q_{\text{Si}} \le Q_{\text{Si},\max} \quad \forall i \in \text{NC} \tag{37}$$

2.13.4 Security constraints

The voltage magnitude of each PQ bus needs to be within specified lower and upper limits, and apparent power flow of each transmission line is restricted by its maximum capacity, as shown in (38).

$$\begin{aligned} V_{\mathrm{Li,min}} \le V_{\mathrm{Li}} \le V_{\mathrm{Li,max}} \quad \forall i \in \mathrm{NPQ} \\ S_{\mathrm{li}} \le S_{\mathrm{li,max}} \quad \forall i \in \mathrm{NTL} \end{aligned} \tag{38}$$

where $V_{\mathrm{Li,\ min}}$ and $V_{\mathrm{Li,\ max}}$ are the lower and upper voltage magnitudes of the ith PQ bus. S_{li} and $S_{\mathrm{li,\ max}}$ are the apparent power flow and maximum apparent power flow capacity of the ith line.

2.13.5 DC transmission link constraints

The lower and upper limits of the DC transmission link parameters are defined as follows.

$$\begin{aligned} i_{d,\min} \le i_d \le i_{d,\max} \\ P_{\mathrm{Dk,min}} \le P_{\mathrm{Dk}} \le P_{\mathrm{Dk,max}} \quad k = 1,2 \\ Q_{\mathrm{Dk,min}} \le Q_{\mathrm{Dk}} \le Q_{\mathrm{Dk,max}} \quad k = 1,2 \\ t_{\mathrm{dk,min}} \le t_{\mathrm{dk}} \le t_{\mathrm{dk,max}} \quad k = 1,2 \\ v_{\mathrm{dk,min}} \le v_{\mathrm{dk}} \le v_{\mathrm{dk,max}} \quad k = 1,2 \\ \alpha_{\min} \le \alpha \le \alpha_{\max} \\ \gamma_{\min} \le \gamma \le \gamma_{\max} \end{aligned} \tag{39}$$

The fitness function of the proposed AC–DC OPF problem including RESs can be identified as in (40).

Where $[f_{\mathrm{obj}}(A,B)$ or $f_{\mathrm{obj}}(A_0,B_0)]$ is defined as objective functions under both pre-contingency and contingency conditions.

Where λ_1, λ_2, λ_3, λ_4, λ_5, λ_6, λ_7, λ_8, λ_9, λ_{10}, λ_{11}, λ_{12}, and λ_{13} are described as the penalty coefficients, which are adjusted according to experience of user. Each of the penalty coefficients is set as $\lambda_1 = 100$, $\lambda_2 = 100$, $\lambda_3 = 250$, $\lambda_4 = 250$, $\lambda_5 = 250$, $\lambda_6 = 250$, $\lambda_7 = 300$, $\lambda_8 = 1000$, $\lambda_9 = 1000$, $\lambda_{10} = 100$, $\lambda_{11} = 100$, $\lambda_{12} = 1000$, and $\lambda_{13} = 1000$.

$$\begin{aligned} J_{\mathrm{fitness}} &= [f_{\mathrm{obj}}(A,B) \text{ or } f_{\mathrm{obj}}(A_0,B_0)] + \mathrm{Penalty} \\ \mathrm{Penalty} &= \lambda_1\left(P_{\mathrm{THG}_1} - P_{\mathrm{THG}_1}^{\mathrm{lim}}\right)^2 + \lambda_2 \sum_{i=1}^{\mathrm{NPQ}} \left(V_{\mathrm{Li}} - V_{\mathrm{Li}}^{\mathrm{lim}}\right)^2 \\ &\quad + \lambda_3 \sum_{i=1}^{\mathrm{NTHG}} \left(Q_{\mathrm{THG}_i} - Q_{\mathrm{THG}_i}^{\mathrm{lim}}\right)^2 + \lambda_4 \sum_{i=1}^{\mathrm{NW}} \left(Q_{\mathrm{WS}_i} - Q_{\mathrm{WS}_i}^{\mathrm{lim}}\right)^2 \\ &\quad + \lambda_5 \sum_{i=1}^{\mathrm{NPV}} \left(Q_{\mathrm{PVS}_i} - Q_{\mathrm{PVS}_i}^{\mathrm{lim}}\right)^2 \\ &\quad + \lambda_6 \sum_{i=1}^{\mathrm{NPPEV}} \left(Q_{\mathrm{PPEVS}_i} - Q_{\mathrm{PPEVS}_i}^{\mathrm{lim}}\right)^2 \\ &\quad + \lambda_7 \sum_{i=1}^{\mathrm{NTL}} \left(S_{\mathrm{li}} - S_{\mathrm{li}}^{\mathrm{lim}}\right)^2 + \lambda_8\left(\alpha - \alpha^{\mathrm{lim}}\right)^2 + \lambda_9\left(\gamma - \gamma^{\mathrm{lim}}\right)^2 \\ &\quad + \lambda_{10}\left(t_r - t_r^{\mathrm{lim}}\right)^2 + \lambda_{11}\left(t_i - t_i^{\mathrm{lim}}\right)^2 + \lambda_{12}\left(v_{\mathrm{dr}} - v_{\mathrm{dr}}^{\mathrm{lim}}\right)^2 \\ &\quad + \lambda_{13}\left(v_{\mathrm{di}} - v_{\mathrm{di}}^{\mathrm{lim}}\right)^2 \end{aligned} \tag{40}$$

3 Wind/PV/PEV uncertainty power models

Wind speed distribution is defined via the Weibull probability density function (PDF) as shown in (41), where ξ and ψ are shape and scale factors (Biswas et al. 2017, 2018b).

$$f_v(v) = \left(\frac{\xi}{\psi}\right) \times \left(\frac{v}{\psi}\right)^{\xi-1} \times \left(\exp\left(-\left(\frac{v}{\psi}\right)^{\xi}\right)\right) \quad 0 < v < \infty \tag{41}$$

Power output of a wind farm is mathematically described as in (42), where p_{wr}, v_{out}, v_r, and v_{in} are, respectively, the rated power, cut-out, rated, and cut-in wind speeds.

$$p_w(v) = \begin{cases} 0 & v < v_{in} \text{ and } v > v_{\mathrm{out}} \\ p_{\mathrm{wr}}\left(\dfrac{v - v_{\mathrm{in}}}{v_r - v_{\mathrm{in}}}\right) & v_{\mathrm{in}} \le v \le v_r \\ p_{\mathrm{wr}} & v_r < v \le v_{\mathrm{out}} \end{cases} \tag{42}$$

When the wind speed is below the cut-in speed, the probability of wind power is presented in (43); when the wind speed is above the cut-out speed, the probability of wind power is shown in (44); and when the wind speed is between the rated and cut-out speeds, the probability of wind power can be defined as in (45).

$$f_w(p_w)\{p_w = 0\} = 1 - e^{-\left(\frac{v_{\mathrm{in}}}{\psi}\right)^{\xi}} + e^{-\left(\frac{v_{\mathrm{out}}}{\psi}\right)^{\xi}} \tag{43}$$

$$f_w(p_w)\{p_w = p_{\mathrm{wr}}\} = e^{-\left(\frac{v_r}{\psi}\right)^{\xi}} - e^{-\left(\frac{v_{\mathrm{out}}}{\psi}\right)^{\xi}} \tag{44}$$

$$\begin{aligned} f_w(p_w) = &\left[\frac{\xi(v_r - v_{\mathrm{in}})}{\psi^{\xi} p_{\mathrm{wr}}}\right] \\ &\times \left(v_{\mathrm{in}} + \left(\frac{p_w}{p_{\mathrm{wr}}}\right)(v_r - v_{\mathrm{in}})\right)^{\xi-1} \times e^{-\left(\frac{v_{\mathrm{in}} + \left(\frac{p_w}{p_{\mathrm{wr}}}\right)(v_r - v_{\mathrm{in}})}{\psi}\right)^{\xi}} \end{aligned} \tag{45}$$

The scale and shape factors are set as 10 and 2 at bus 8 on the IEEE 30-bus test system. The wind power amounted to the summation of the power outputs from 20 turbines at bus 8, with the rated power of 3 MW each. The wind speed values were determined as $v_{\mathrm{in}} = 3$ m/s, $v_r = 16$ m/s, and $v_{\mathrm{out}} = 25$ m/s (Biswas et al. 2017). After Monte Carlo simulation with a sample size of 8000 had been run, the frequency distribution of wind speed and the Weibull fitting were determined, and shown in Fig. 5.

The power output of PV systems can be mathematically expressed as a function of solar irradiation. The distribution of solar irradiation is generally modeled using the Log-normal PDF (Biswas et al. 2017, 2018b). The probabilistic model and power output of the PV system can be defined as follows.

$$f_{G_{\mathrm{pv}}}(G_{\mathrm{pv}}) = \frac{1}{G_{\mathrm{pv}}\Omega\sqrt{2\pi}} e^{\left(\frac{-(\ln G_{pv} - \eta)^2}{2\Omega^2}\right)} \quad \text{for } G_{\mathrm{pv}} > 0 \tag{46}$$

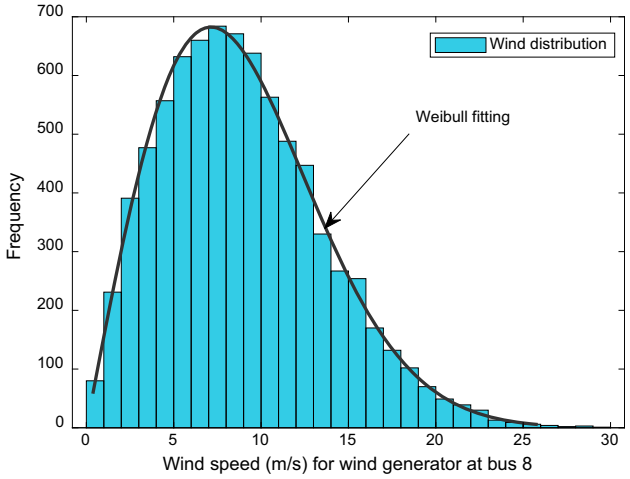


Fig. 5 Wind speed distribution at bus 8

$$P_{\mathrm{PVo}} = \begin{cases} P_{\mathrm{PVrate}} \times \left(\dfrac{G_{\mathrm{pv}}}{G_{\mathrm{pvstd}} \times Rc} \right) & \text{for } 0 < G_{\mathrm{pv}} < \mathrm{Rc} \\ P_{\mathrm{PVrate}} \times \left(\dfrac{G_{\mathrm{pv}}}{G_{\mathrm{pvstd}}} \right) & \text{for } G_{\mathrm{pv}} \geq \mathrm{Rc} \end{cases} \tag{47}$$

where η and Ω are, respectively, the mean and standard deviation values of the Lognormal PDF, which are set as 5.2 and 0.6 at bus 11, 5 and 0.6 at bus 13 of the IEEE 30-bus system. G_{pv} and P_{pvrate} are, respectively, the probability value of solar irradiance and rated power of the PV system, which were set as 50 MW at bus 11 and 26.4 MW at bus 13 of the IEEE 30-bus system.

G_{pvstd} is the solar irradiance value under standard environmental conditions, which was set at 1000 W/m^2, and the Rc value was set at 120 W/m^2. The frequency distributions of solar irradiance for the PV system and the Lognormal fitting were determined, and are shown in Fig. 6a and b.

Recently, the representation of PEV load has been used as research subject in the literature by the researchers. Qian et al. proposed a method to represent modeling of load demand due to electric vehicle (EV) battery charging in distribution systems. The authors considered the probabilistic conditions, which are the time of switching on an individual charger and behavior of vehicle usage (Qian et al. 2011). Zeng et al. presented the hybrid probabilistic possibilistic method for capacity credit evaluation of demand response under the different cases on a modified IEEE-RTS system. The authors have shown the practicality of the proposed method for estimating the capacity credit evaluation of demand response in smart grid system (Zeng et al. 2018). In another study, Zeng et al. used a new method to manage the stochastic energy flow analysis of integrated energy systems. This method is named as Z-number-based technique by the authors. To show the usability of this method, the simulation studies are made under the different scenarios (Zeng et al. 2019). Sarić and Stanković focused on an application of interval analysis and optimization to electric energy markets on 68-node New England/New York interconnected power system (Sarić and Stanković 2006).

In our study, the PEVs were modelled by considering their charging and discharging operation situations, and considered as ideal batteries. The Normal PDF was used as the probability function for the modeling of the PEV systems (Zhao et al. 2012; Arevalo et al. 2019) as follows.

$$f_{P_{\mathrm{pev}}}(P_{\mathrm{pev}}) = \frac{1}{\sqrt{2\pi\varphi^2}} \exp\left(-\left(\frac{P_{\mathrm{pev}} - \vartheta}{\sqrt{2}\varphi} \right)^2 \right) \tag{48}$$

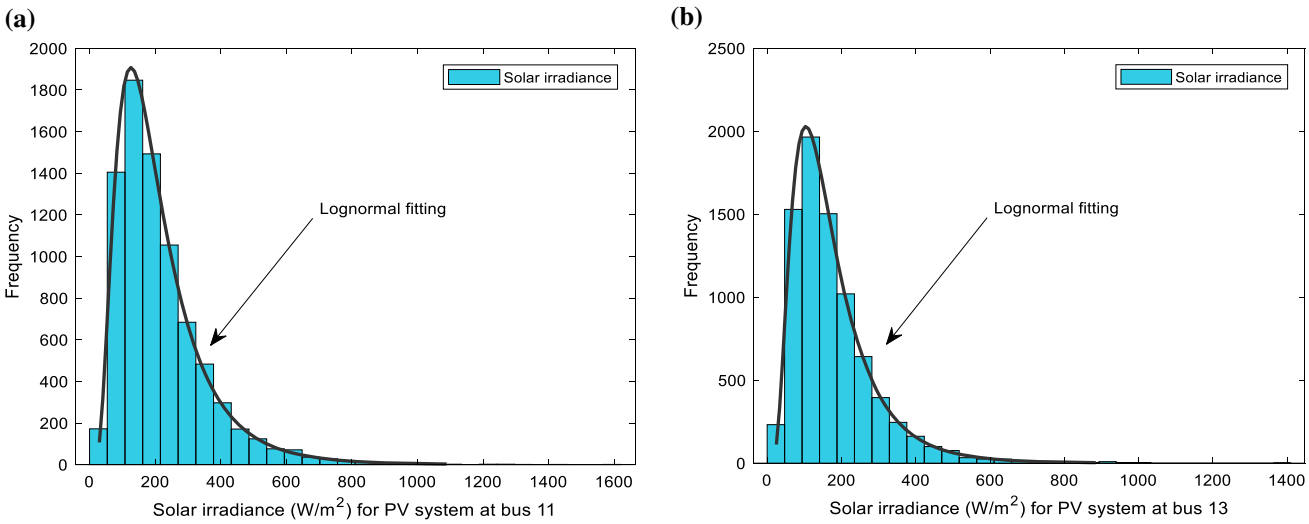


Fig. 6 Solar irradiance distribution for PV systems at buses 11 and 13

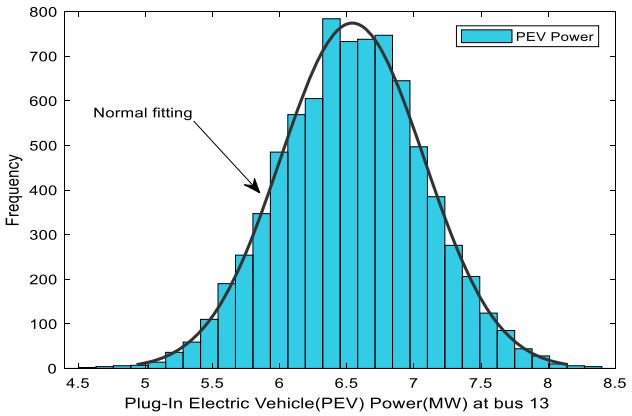


Fig. 7 PEV power distribution for PEV system at bus 13

where P_{pev} expresses the available power of the PEV, ϑ and $\varnothing$ are, respectively, the mean and standard deviation values of the Normal PDF, which were set as 6.54 and 0.54 at bus 13 in the IEEE 30-bus test system. In addition, the charge situation attracted a negative power or load from the system, and the discharge situation provided a positive power to the system (Arevalo et al. 2017; 2019). In this study, the active power limits of the PEVs were set as -8 MW and 13.6 MW based on Ref. (Arevalo et al. 2017). Firstly, the Monte Carlo simulation with a sample size of 8000 was run. Later, Normal fitting, and frequency distribution of the PEV are obtained as shown in Fig. 7.

4 Symbiotic organisms search algorithm

The SOS optimization method is one of the new heuristic algorithms inspired by the symbiotic interaction phenomena in ecosystems (Cheng and Prayogo 2014). The symbiotic relationship is defined as the relationship between the organisms in the ecosystem, with each organism in the ecosystem representing a candidate solution in the search space of an optimization problem. At the beginning of the algorithm, the initial population or ecosystem is randomly constituted for the candidate solutions of problem. First, the organisms are created for the candidate solutions and the candidate solution vector is generated depending on the limit values of the variables. The generation of the ecosystem and organisms is shown in Fig. 8 (Duman 2017). The SOS algorithm has a simple structure and includes the three phases of Mutualism, Commensalism, and Parasitism. The algorithm and the developed version of the SOS are used to solve many optimization problems in various engineering and scientific fields including optimal power flow problems with FACTS devices along with radial distribution network planning, neural network training, load frequency control and traveling salesman problems (Ezugwu and Prayogo 2019).

4.1 Mutualism phase

The mutualism phase of the SOS algorithm can be defined depending on the symbiotic relationships between two organisms that are benefited in the ecosystem. X_m and X_n are, respectively, the organisms in the ecosystem, and X_n randomly chosen from the ecosystem to interact with organism X_m. In order to ensure the survival of both organisms in the ecosystem, a relationship is introduced by

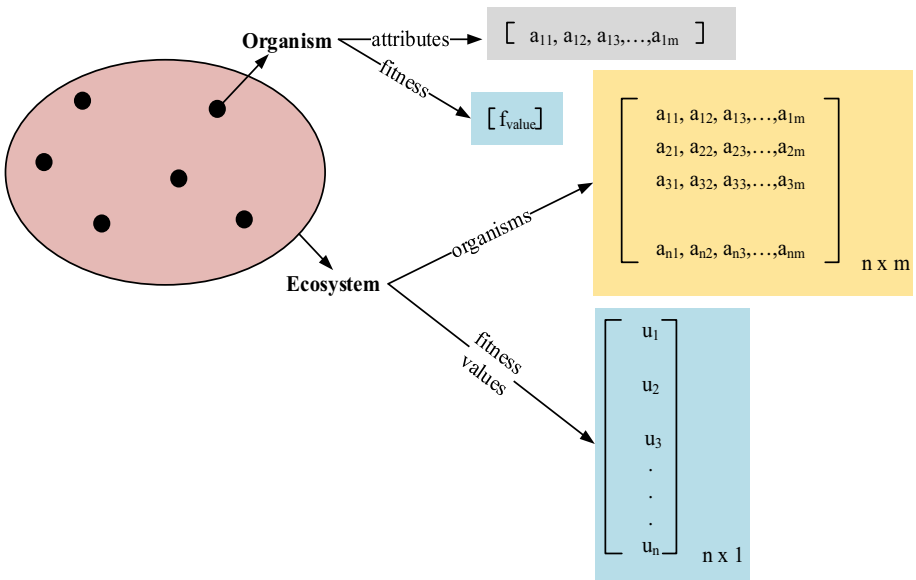


Fig. 8 The relationship model of organisms and ecosystem (Duman 2017)

the organisms X_m and X_n which is mathematically described as follows. The new candidate solutions in the ecosystem are obtained as X_{mnew} and X_{nnew}, which are given in (49).

$$\begin{aligned} X_{\text{mnew}} &= X_m + \text{rand}(0,1) \times \left(X_{\text{best}} - \boldsymbol{Mut_Vect} \times B_{f1}\right) \\ X_{\text{nnew}} &= X_n + \text{rand}(0,1) \times \left(X_{\text{best}} - \boldsymbol{Mut_Vect} \times B_{f2}\right) \\ \boldsymbol{Mut_Vec} &= \frac{X_m + X_n}{2} \end{aligned} \tag{49}$$

where rand(0, 1) is a random number between 0 and 1, B_{f1} and B_{f2} are defined as benefit factors, which show the beneficial relationship of organisms in the ecosystem enabling the generation of new organisms. The ***Mut_Vect*** and X_{best} are, respectively, identified as the relationship between X_m and X_n organisms, and the best solution in the ecosystem. The organisms update with the new candidate solutions when these have better fitness value than the previous fitness ones. Otherwise, the new candidate solutions are not used to find the optimal solution in search space or ecosystem.

4.2 Commensalism phase

The commensalism phase of the SOS algorithm is identified as the symbiotic relationship between two different organisms, where X_n is the nth organism of the ecosystem, chosen randomly from the ecosystem to interact with organism X_m. The organism X_m benefits from the interaction, whereas the other organism shows unaffected behavior. The new candidate solution in the ecosystem is defined as follows.

$$X_{\text{mnew}} = X_m + \text{rand}(-1,1) \times (X_{\text{best}} - X_n) \tag{50}$$

The old candidate solution in this phase updated with the new candidate solution when the new candidate solution has a better fitness value than the previous one. Otherwise, the new candidate solution is not used to find the optimal solution in the ecosystem.

Symbiotic Organisms Search Algorithm

```
1. Start
2. Create initial a random population in ecosystem
3.      // Initialization
4.          for i=1:Eco_size
5.              Compute the fitness value of each organisms, Xi
6.              Identify best organism (Xbest)
7.          end for
8. while stopping criteria is not satisfied do
9.      for m=1:Eco_size
10.         // Mutualism Phase
11.             Select one organism, (Xn) and Xm ≠ Xn
11.             Determine mutual vector Mut_vect=(Xm+Xn)/2  and benefit factors (Bf1, Bf2)
12.             Then Xm_new=Xm + rand(0,1) × (Xbest -  Mut_vect × Bf1)
                     Xn_new=Xn + rand(0,1) × (Xbest -  Mut_vect × Bf2)
13.                 if    f(Xm_new)<f(Xm)
14.                     Xm ⟵ Xm_new
15.                 end if
16.                 if    f(Xn_new)<f(Xn)
17.                     Xn ⟵ Xn_new
18.                 end if
19.         // Commensalism Phase
20.             Select one organism, (Xn) and Xm ≠ Xn
21.             Determine modify organism  Xm_new=Xm + rand(-1,1) × (Xbest - Xn)
23.                 if    f(Xm_new)<f(Xm)
24.                     Xm ⟵ Xm_new
25.                 end if
26.         // Parasitism Phase
27.             Select one organism, (Xn) and Xm ≠ Xn
28.             Identify a Parasite Vector (parasite_vect) from the organism (Xm)
29.                 if    f(Xp_new)<f(Xn)
30.                     Xn ⟵ Xp_new
31.                 end if
32.     end for
33. end while
34. End
```

Fig. 9 The pseudocode of SOS algorithm

4.3 Parasitism phase

This phase of the SOS algorithm can be explained as the symbiotic relationship between two different organisms. In a parasitism phase, the organism X_n is selected from the ecosystem. A parasite vector (parasite_vect) is constituted from the organism X_m. The fitness value of the parasite_vect is computed, and if this fitness value is better than that of organism X_n, the parasite_vect replaces organism X_n in the ecosystem. Otherwise, the parasite vector is not used to find the optimal solution in the ecosystem.

The main structure of the SOS algorithm is summarized via the pseudocode in Fig. 9.

4.4 The SOS algorithm applied to security-constrained AC–DC OPF problem with Wind, PV and PEV systems

The application of the SOS algorithm to the proposed security-constrained AC–DC OPF problem incorporating wind, PV and PEV systems is explained step-by-step in Sect. 4.4.

- *Step 1* In this step, read the all of the parameters belonging to test system, and specify the number of iteration, size of population, and number of dimension of the SOS algorithm. In addition to this step, the independent variables of the proposed problem are generated within the specified limit values for the beginning population.

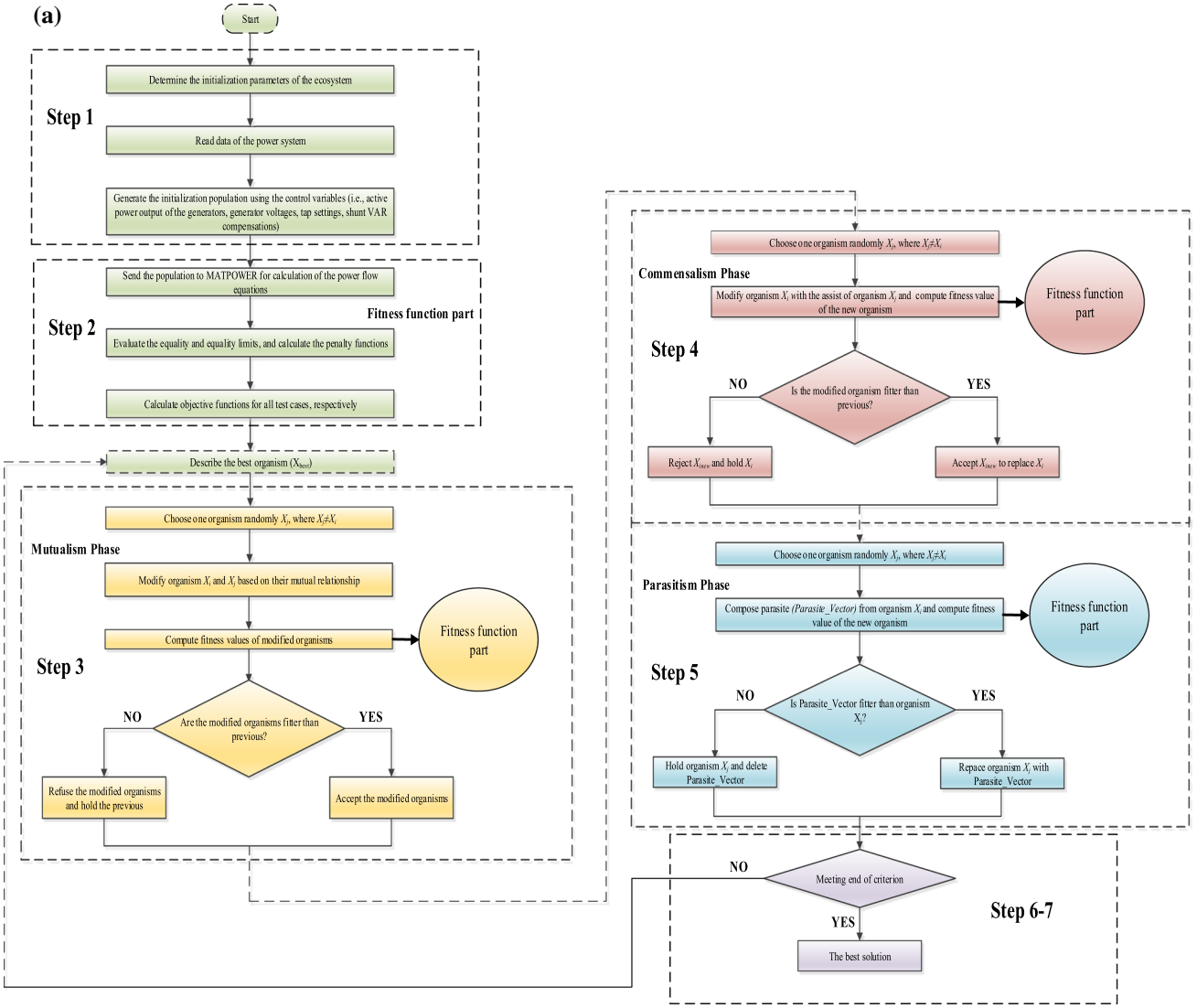


Fig. 10 Application of SOS algorithm to OPF problem: **a** Flowchart of algorithm, **b** Fitness function part

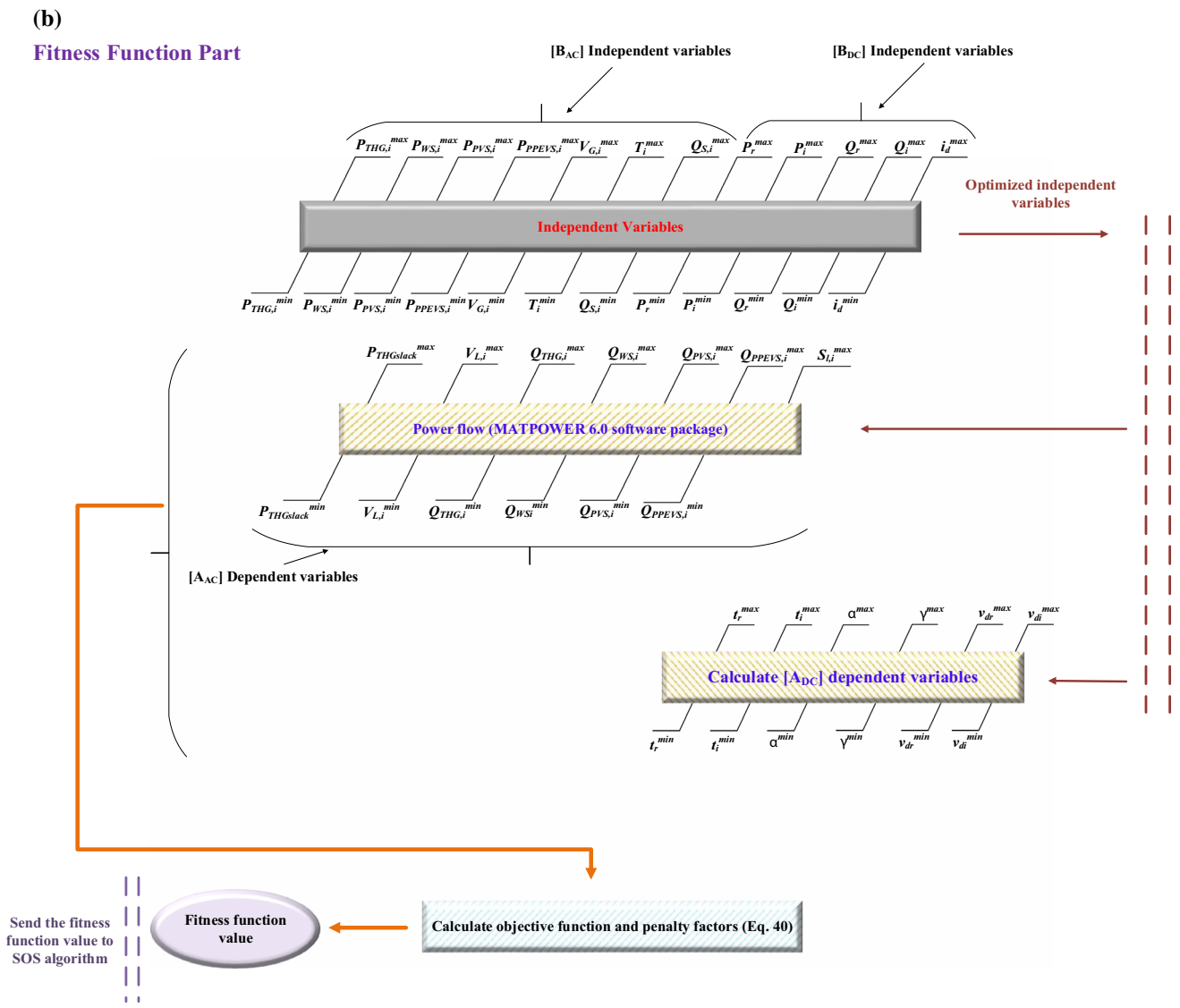


Fig. 10 continued

Table 1 Setting parameters of all optimization algorithms

Algorithms	Parameters settings
SOS	Ecosystem size = 50 Iteration = 300
ABC	Colony size = 50 number of food sources (SN) = colony size/2 limit = D * SN Iteration = 300
ICA	Population size = 50 Iteration = 300 beta = 1.5 zeta = 0.2 gamma = 0.5
MSA	Population size = 50 Iteration = 300
SFLA	Population size = 50 Iteration = 300
GA	Population size = 50 Iteration = 300 Crossover Percentage = 0.8 Mutation Rate = 0.1
PSO	Swarm size = 50 cognitive constant = 2 social constant = 2 inertia weight (\omega) linearly decreases from 0.9 to 0.4 Iteration = 300

- *Step 2* The generated independent variables in the beginning population according to limit values are sent to Newton–Raphson power flow and objective function to calculate the fitness function. Newton–Raphson is run to control that the dependent variables, and the inequality constraints are within the limits or not. The

best organism of the algorithm is determined in the population.

- *Step 3* According to mutualism phase operator, the produced new candidate solution is sent to the objective function to compute fitness function of the problem. The dependent variables and the inequality constraints are checked depending on the obtained results from the Newton–Raphson method, and then the value of the new candidate solution is compared to previous fitness values.
- *Step 4* The flow process in Step 3 is valid for commensalism phase operator.
- *Step 5* The flow process in Step 3 is valid for parasitism phase operator.
- *Step 6* Update the fitness value and the values of the independent variables.
- *Step 7* Go to Step 3 until the maximum number of function evaluations is reached.

The flow diagram showing the application of the SOS algorithm to the intended OPF problem is shown in Fig. 10. Figure 10a shows the implementation steps of the algorithm as described above. Figure 10b explains in detail the application process of the fitness function in the problem.

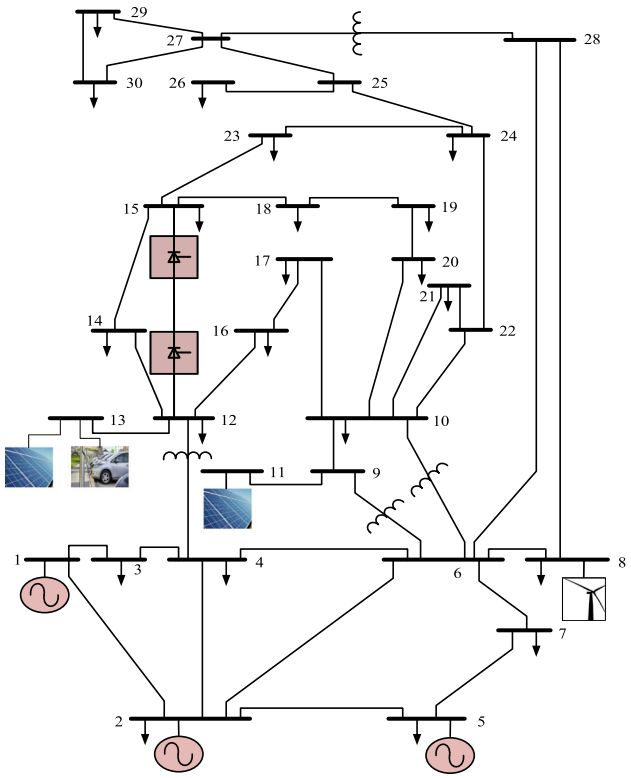


Fig. 11 Modified IEEE 30-bus test system with RESs and HVDC systems

5 Simulation studies

5.1 Experimental settings

The power flow calculations of the OPF problem with RESs and two terminal HVDC systems are carried out via MATPOWER 6.0 (Zimmerman et al. 2011; MATPOWER http://www.pserc.cornell.edu/matpower/). In this study, the algorithms used were run 30 times for all the test cases in order to obtain statistically results valid results. All optimization algorithms were run using an Intel(R) Core(TM) i7-8750H CPU@2.20 GHz with 16 GB of RAM and × 64-based processor. The setting parameters belonging to themselves of all used optimization algorithms in this paper are given in Table 1. The information given in their original studies in which the algorithms were introduced was taken as the reference to determine the parameter settings. Moreover, the maximum iteration number was used as the stopping criteria and the number of population size (Nps) of algorithms is identified as the same value.

5.2 Simulation results

In this study, the SOS, ABC, ICA, MSA, SFLA, GA, and PSO optimization algorithms were used to solve the AC–DC OPF problem of an IEEE 30-bus and IEEE 57-bus

Table 2 Fuel and emission coefficients of thermal generating units

Units	x ($/h)	y ($/MWh)	z ($/MW^{2}h)	d ($/h)	e (rad/MW)	σ (ton/h)	β (ton/MWh)	τ (ton/MW^{2}h	ω (ton/h)	μ (1/MW)	Prohibited zones
IEEE 30-bus test system											
P_{THG1}	0	2.00	0.00375	18	0.037	0.04091	− 0.05554	0.06490	0.000200	2.857	[55–66], [80–120]
P_{THG2}	0	1.75	0.01750	16	0.038	0.02543	− 0.06047	0.05638	0.000500	3.333	[21–24], [45–55]
P_{THG5}	0	1.00	0.06250	14	0.040	0.04258	− 0.05094	0.04586	0.000001	8.000	[30–36]

Table 3 Parameters of the test systems

Characteristics	IEEE 30-bus system	
	Number	Details
Bus	30	IEEE 30-bus test system data http://labs.ece.uw.edu/pstca/pf30/pg_tca30bus.htm
Branch	41	IEEE 30-bus test system data http://labs.ece.uw.edu/pstca/pf30/pg_tca30bus.htm
Thermal generators	3	Buses: 1, 2 and 5
Slack generator	1	Buses: 1
Wind farm	1	Buses: 8
PV system	1	Buses: 11 and 13
PEV system		Buses: 13
Transformer	4	Branches: 11, 12, 15 and 36
Capacitor bank	2	Buses: 10, 24
Independent variable	17	–
Load bus voltage limit	24	[0.95–1.05] p.u

test systems while considering uncertainties of wind, PV, and PEV systems. The test system parameters are taken from Refs. (Duman 2017; Chaib et al. 2016; http://labs.ece.uw.edu/pstca/pf30/pg_tca30bus.htm; http://labs.ece.uw.edu/pstca/pf57/pg_tca57bus.htm), and Table 2 shows fuel cost coefficients, emission coefficients, and POZs of the thermal generating units. The total active and reactive power base loads of the IEEE 30-bus were 2.834 and 1.262 p.u. at the 100 MVA base. The total active and reactive power base loads were 12.508 and 3.364 p.u. for IEEE 57-bus test system at the 100-MVA base. Reactive power is one of the most important parameters of OPF problems in modern power systems. In this study, reactive power limits of wind, PV and PEV systems were $-0.4 \times P_{\text{res},\,i}^{\max}$ p.u. and $0.5 \times P_{\text{res},\,i}^{\max}$ p.u. (Biswas et al. 2017, 2018b). $P_{\text{res},\,i}^{\max}$ was the maximum active power of RESs (wind, PV, and PEV systems). The single line diagram of the modified IEEE 30-bus test system with RESs, and a two terminal HVDC system is shown in Fig. 11.

Table 4 Upper and lower limits of dependent variables

Variables (A_{AC})	$A_{AC,\,min}$	$A_{AC,\,max}$	Variables (A_{DC})	$A_{DC,\,min}$	$A_{DC,\,max}$
P_{THG1} (MW)	50	200	t_r	1.0	1.10
$V_{L,\,NPQ}$	0.95	1.05			
Q_{THG1} (MVAr)	− 20	150	t_i	1.0	1.10
Q_{THG2} (MVAr)	− 20	60			
Q_{THG5} (MVAr)	− 15	62.5	$\alpha(^\circ)$	9.74	22.91
Q_{WS1} (MVAr)	− 24	30	$\gamma\ (^\circ)$	8.59	22.91
Q_{PVS} (MVAr)	− 20	25	v_{dr}	1.0	1.5
$Q_{PVS+PEV}$ (MVAr)	− 16	20	v_{di}	1.0	1.5

Table 5 Upper and lower limits of independent variables

Variables (B_{AC})	$B_{AC,\,min}$	$B_{AC,\,max}$	Variables (B_{DC})	$B_{DC,\,min}$	$B_{DC,\,max}$
P_{THG2} (MW)	20	80	Pr (p.u)	0.1	1.5
P_{THG5} (MW)	15	50			
P_{WS1} (MW)	0	60			
P_{PVS} (MW)	0	50	Pi (p.u)	0.1	1.5
$P_{PVS+PEV}$ (MW)	− 8	40			
V_{G1} (p.u.)	0.95	1.10			
V_{G2} (p.u.)	0.95	1.10	Qr (p.u)	0.05	0.75
V_{G5} (p.u.)	0.95	1.10			
V_{G8} (p.u.)	0.95	1.10			
V_{G11} (p.u.)	0.95	1.10	Qi (p.u)	0.05	0.75
V_{G13} (p.u.)	0.95	1.10			
T_{11} (p.u.)	0.90	1.10			
T_{12} (p.u.)	0.90	1.10	i_d	0.1	1.0
T_{15} (p.u.)	0.90	1.10			
T_{36} (p.u.)	0.90	1.10			
Q_{C10} (MVAr)	0	30			
Q_{C24} (MVAr)	0	30			

Table 6 Cost model coefficient of renewable energy sources

Cost coefficients of wind power ($/MW)				Cost coefficients of PV system ($/MW)				Cost coefficients of combined PV and PEV system ($/MW)			
Bus No.	ww, i	$C_{Ow,\ i}$	$C_{Uw,\ I}$	Bus No.	pv, i	$C_{Opv,\ i}$	$C_{Upv,\ i}$	Bus No.	pev, i	$C_{Oppev,\ i}$	$C_{Uppev,\ i}$
IEEE 30-bus test system											
Bus 8	1.8	3	1.5	Bus 11 and 13	1.7	3	1.6	Bus 13	1.6	3	1.5
Cost coefficients of wind power ($/MW)				Cost coefficients of wind power ($/MW)				Cost coefficients of combined PV and PEV system ($/MW)					
Bus No	ww, i	$C_{Ow,\ i}$	$C_{Uw,\ I}$	Bus No.	ww,i	$C_{Ow,\ i}$	$C_{Uw,\ I}$	Bus No.	pev, i	pv, i	$C_{Oppev,\ i}$	$C_{Uppev,\ i}$
IEEE 57-bus test system												
Bus 6	3.2	6	3	Bus 9	3.5	6	3	Bus 2	3.2	3.4	6	3

Table 3 gives a summary of the parameters of test system, and the upper and lower limits of dependent and independent variables are, respectively, given in Tables 4 and 5. Table 4 describes the limits values of the dependent variables in both AC and DC systems according to Refs. (Kılıç et al. 2014; Biswas et al. 2017, 2018b; Chaib et al. 2016; http://labs.ece.uw.edu/pstca/pf30/pg_tca30bus.htm). Table 5 defines the limits values of the independent variables, which are optimized by the heuristic algorithms in both AC and DC systems according to Refs. (Kılıç et al. 2014; Biswas et al. 2017, 2018b; Chaib et al. 2016; http://labs.ece.uw.edu/pstca/pf30/pg_tca30bus.htm). Table 6 shows the direct, overestimation and underestimation cost coefficients of the wind, PV and PEV systems.

In order to evaluate the performances of the SOS and other methods, the modified IEEE test systems with RESs and HVDC systems were tested via the multiple study cases described below.

Test system 1 Modified IEEE 30-bus test system with RESs and HVDC systems.

- *Case 1* An OPF problem with a quadratic cost function for thermal generating units, and a cost model of wind, PV, and combined PV and PEV energy sources
- *Case 2* An OPF problem with cost function and valve point effect for thermal generating units, and a cost model of wind, PV, and combined PV and PEV energy sources
- *Case 3* An OPF problem with cost function and POZs for thermal generating units, and a cost model of wind, PV, and combined PV and PEV energy sources
- *Case 4* An OPF problem with a cost function as well as emission and tax for thermal generating units, and a cost model of wind, PV, and combined PV and PEV energy sources
- *Case 5* An OPF problem with improvement of voltage stability considering thermal generating units, and a cost model of wind, PV, and combined PV and PEV energy sources
- *Case 6* An OPF problem with voltage deviation considering thermal generating units, and a cost model of wind, PV, and combined PV and PEV energy sources
- *Case 7* A security-constrained OPF problem with selected N-1 contingency conditions

Test system 2 Modified IEEE 57-bus test system with RESs and HVDC systems.

- *Case 8* The OPF problem with a quadratic cost function for thermal generating units, and a cost model of wind, PV, and combined PV and PEV energy systems
- *Case 9* The OPF problem with cost function and valve point effect for thermal generating units, and a cost model of wind, PV, and combined PV and PEV energy systems
- *Case 10* The OPF problem with a cost function as well as emission and tax for thermal generating units, and a cost model of wind, PV, and combined PV and PEV energy systems

5.2.1 Test system 1

Case 1 Minimization of total cost of thermal and wind-PV-PEV systems The minimization of the total cost considering the quadratic cost function of the thermal generators, the cost model of RESs and PEV systems were studied in Case

Table 7 The simulation results of SOS algorithm for all cases

Parameters	Case 1	Case 2	Case 3	Case 4	Case 5	Case 6	Case 7.1 (line outage (15–23))	Case 7.2 (line outage (12–15))	Case 7.3 (line outage (6–28))
P_{THG1} (MW)	164.0899	141.0806	164.2982	162.2689	123.4320	50.6136	163.8934	164.5089	163.3454
P_{THG2} (MW)	45.3520	54.8992	44.9991	46.2697	24.4530	79.8570	45.6656	45.6498	45.8986
P_{THG5} (MW)	20.3707	20.0192	20.3695	20.6935	48.6967	37.3233	20.4303	20.5255	20.2895
P_{WS1} (MW)	36.8958	45.2180	36.7931	37.2852	58.3178	40.3396	36.6925	36.6725	36.9067
P_{PV} (MW)	12.6258	15.9044	12.6242	12.6428	41.4712	49.9920	12.6377	12.6195	12.6137
P_{PV+PEV} (MW)	12.1718	13.2691	12.4271	12.2483	− 7.5998	29.3637	12.3271	12.1163	12.6170
V_1 (p.u.)	1.0792	1.0762	1.0811	1.0808	1.0806	1.0005	1.0801	1.0815	1.0804
V_2 (p.u.)	1.0618	1.0613	1.0627	1.0633	1.0755	1.0002	1.0631	1.0632	1.0634
V_5 (p.u.)	1.0319	1.0319	1.0319	1.0329	1.0678	1.0138	1.0330	1.0339	1.0339
V_8 (p.u.)	1.0398	1.0429	1.0400	1.0418	1.0527	1.0047	1.0424	1.0413	1.0397
V_{11} (p.u.)	1.0530	1.0811	1.0525	1.0439	1.0735	1.0232	1.0800	1.0922	1.0956
V_{13} (p.u.)	1.0690	1.0667	1.0661	1.0603	1.0338	1.0334	1.0595	1.0463	1.0609
T_{11} (p.u.)	1.0147	1.0205	1.0183	1.0903	1.1000	1.0353	1.0306	1.0480	1.0366
T_{12} (p.u.)	0.9909	0.9711	0.9779	0.9189	0.9000	1.0054	0.9796	0.9375	0.9362
T_{15} (p.u.)	0.9732	0.9698	0.9673	0.9579	0.9017	0.9831	0.9570	0.9563	0.9616
T_{36} (p.u.)	0.9949	0.9959	0.9955	0.9942	0.9754	0.9833	0.9698	0.9691	0.9773
Q_{C10} (MVAr)	27.2904	17.8900	25.1363	29.7313	14.0547	28.7399	22.4425	18.8274	10.4079
Q_{C24} (MVAr)	11.9771	11.8877	11.8593	11.8796	5.9745	17.1347	11.5300	17.4060	15.3415
Pr (p.u)	0.1305	0.1308	0.1310	0.1304	0.2066	0.1621	0.1308	0.2022	0.1320
Pi (p.u)	0.1305	0.1308	0.1309	0.1304	0.2065	0.1620	0.1308	0.2022	0.1320
Qr (p.u)	0.0565	0.0568	0.0549	0.0569	0.0500	0.0592	0.0547	0.0500	0.0557
Qi (p.u)	0.0500	0.0500	0.0500	0.0500	0.0502	0.0500	0.0500	0.0500	0.0501
i_d	0.1000	0.1002	0.1001	0.1000	0.1486	0.1200	0.1000	0.1381	0.1010
t_r	1.0024	1.0033	1.0000	1.0035	1.0095	1.0569	1.0001	1.0638	1.0004
t_i	1.0002	1.0000	1.0025	1.0002	1.0088	1.0462	1.0020	1.0934	1.0001
$\alpha(^\circ)$	22.6788	22.7697	21.9907	22.8733	11.7222	19.0854	21.9435	12.2761	22.1416
$\gamma(^\circ)$	20.5034	20.4607	20.4490	20.5196	12.6028	16.4808	20.4546	12.9965	20.3257
v_{dr}	1.3045	1.3049	1.3078	1.3042	1.3905	1.3505	1.3084	1.4642	1.3069
v_{di}	1.3042	1.3045	1.3075	1.3038	1.3900	1.3501	1.3081	1.4637	1.3066
Q_{THG1} (MVAr)	0.0888	− 0.8955	3.1256	1.7430	− 11.2199	− 18.8787	− 0.2879	3.0969	0.2635
Q_{THG2} (MVAr)	18.2256	16.1298	18.3873	18.8369	41.4791	− 16.1069	19.7871	17.6586	20.0458
Q_{THG5} (MVAr)	25.8426	25.3170	25.5315	25.1107	41.1447	52.9024	25.1067	26.4949	26.4885
Q_{WS1} (MVAr)	26.7898	28.0255	28.1538	27.6493	29.5160	29.2828	28.4206	27.9632	29.9413
Q_{PV} (MVAr)	4.8910	16.4248	5.4514	10.6345	24.9927	13.9424	17.1758	24.5039	24.4267
Q_{PV+PEV} (MVAr)	14.6703	12.8751	12.3479	7.8881	− 11.5006	19.8340	7.2928	− 2.5743	8.3877
	769.5928	**798.8588**	**769.8551**	**769.9865**	933.3314	921.4875	**770.4154**	**771.5253**	**770.2653**

Table 7 (continued)

Parameters	Case 1	Case 2	Case 3	Case 4	Case 5	Case 6	Case 7.1 (line outage (15–23))	Case 7.2 (line outage (12–15))	Case 7.3 (line outage (6–28))
Total Cost ($/h)									
Emission (t/h)	0.1922	0.1496	0.1927	**0.1882**	0.1219	0.0805	0.1918	0.1931	0.1906
Carbon Tax ($/h)	3.8446	2.9911	3.8539	**3.7634**	2.4375	1.6101	3.8355	3.8619	3.8124
P_{loss} (MW)	8.1026	6.9871	8.1079	8.0051	5.3635	4.0844	8.2432	8.6861	8.2675
VD (p.u.)	0.8877	0.9078	0.8746	0.8709	0.9166	**0.12445**	0.9245	0.8285	0.8781
L-index	0.1390	0.1385	0.1391	0.1389	**0.13601**	0.1505	**0.1449**	**0.1489**	**0.1505**

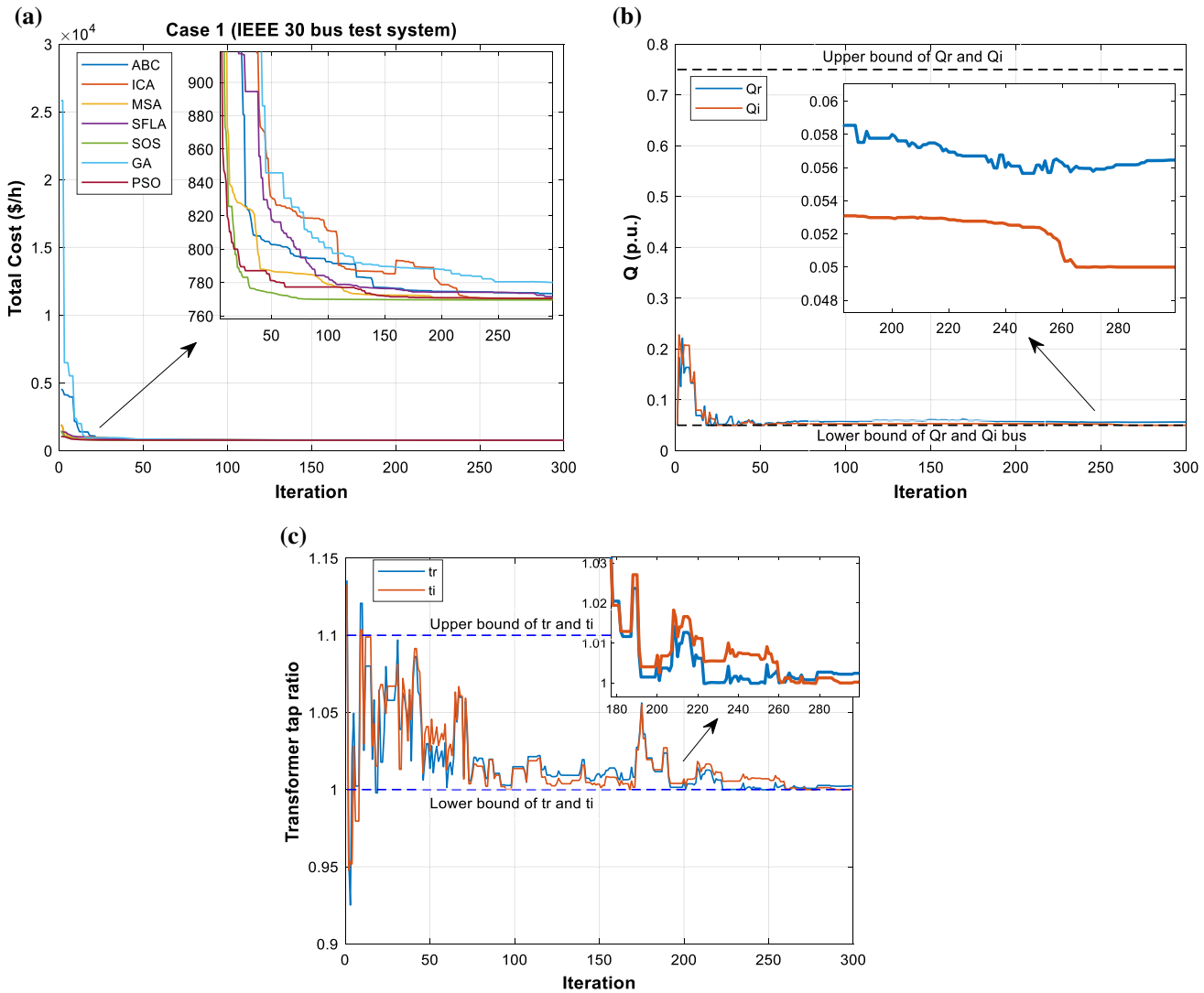


Fig. 12 Convergence curves of all algorithms, (**b**) reactive power (**c**) transformer tap ratio variations in rectifier and inverter sides (for Case1)

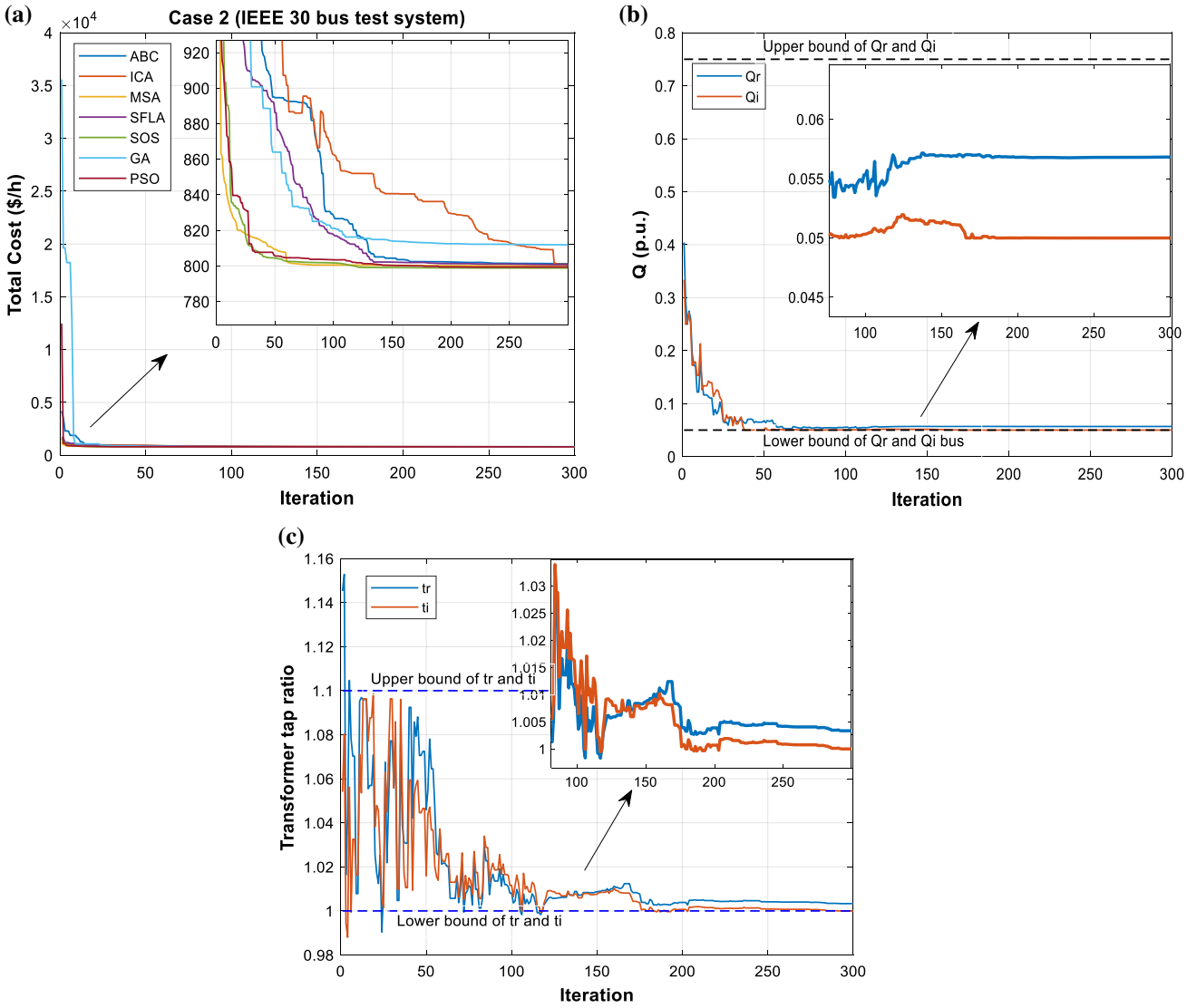


Fig. 13 Convergence curves of all algorithms, (**b**) reactive power (**c**) transformer tap ratio variations in rectifier and inverter sides (for Case2)

1. The formulation of this case is given as an objective function in (24). Table 7 shows the obtained optimal values of the independent variables from the SOS algorithm for all cases. Total cost values from the proposed SOS, ABC, ICA, MSA, SFLA, GA and PSO methods were 769.5928 $/h, 773.4497 $/h, 770.448 $/h, 770.6341 $/h, 771.6566 $/h, 780.1213 $/h, and 770.5165, respectively. The simulation result from the SOS algorithm was 3.8569 $/h, 0.8552 $/h, 1.0413 $/h, 2.0638 $/h, 10.5285 $/h, and 0.9237 $/h lower than the simulation results from ABC, ICA, MSA, SFLA, GA and PSO algorithms, respectively.

Figure 12a shows the convergence curves of the fitness function value of all optimization algorithms for Case 1. It is obviously shown that the proposed SOS algorithm converges to the optimal solution of the problem faster than the other algorithms. Figure 12b and c shows the reactive power and transformer tap ratio variations at both rectifier and inverter sides throughout the optimization period.

Case 2 Minimization of total cost with valve point effect of thermal and wind-PV-PEV systems For Case 2, the cost models for minimizing total cost considering quadratic cost function with the valve point effect of the thermal generating units, RES and PEV systems, the formulation in (25) was used as the objective function. The obtained simulation result of the SOS algorithm was 798.8588 $/h, which was 0.30109%, 0.26344%, 0.15425%, 0.22168%, 1.60854%, and 0.06985% lower than ABC, ICA, MSA SFLA, GA and PSO algorithms. Figure 13a shows the convergence curves of the optimization algorithms for this case and clearly indicates that the SOS algorithm effectively converges to

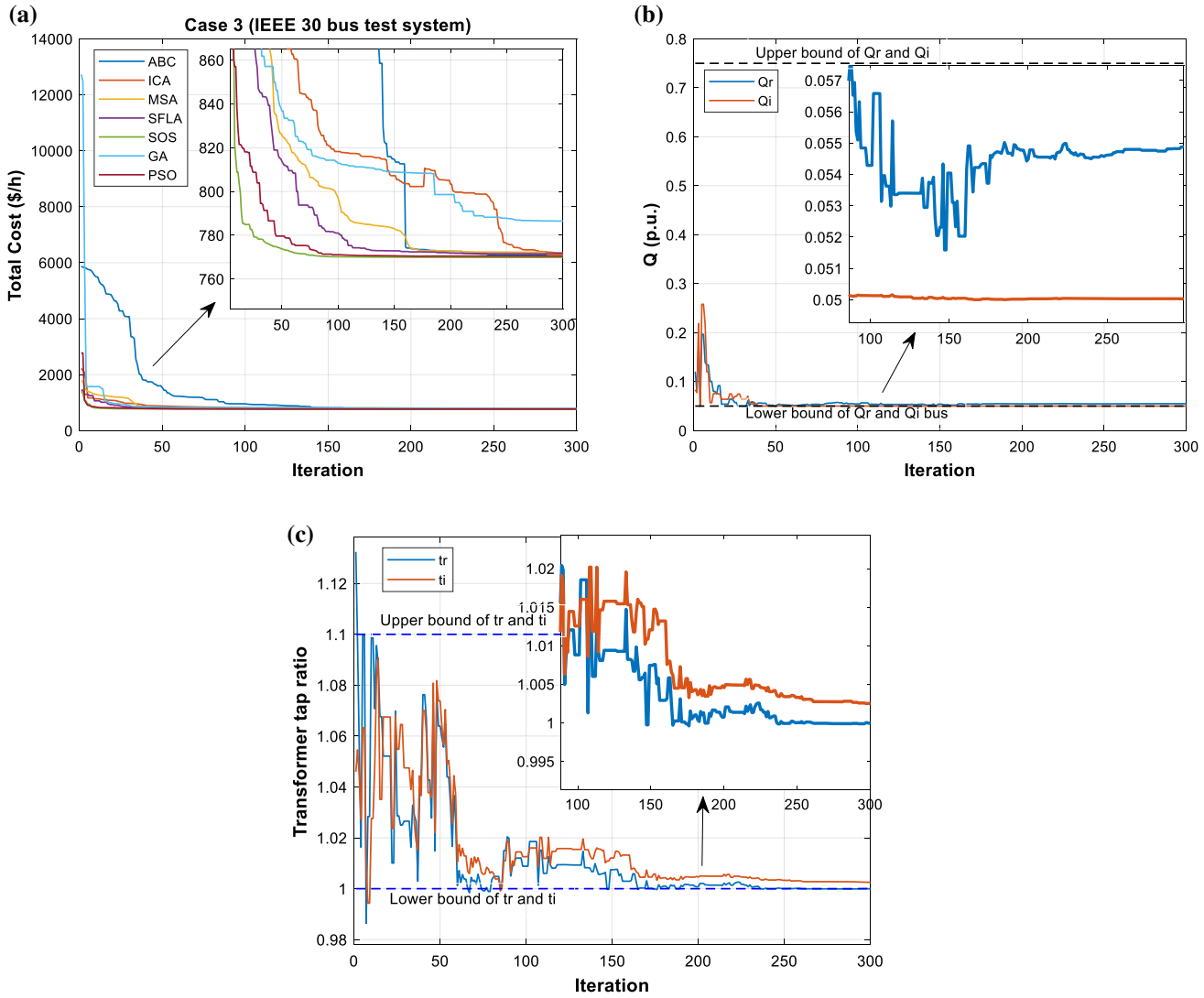


Fig. 14 Convergence curves of all algorithms, (**b**) reactive power (**c**) transformer tap ratio variations in rectifier and inverter sides (for Case3)

the optimal solution compared to the other algorithms. The reactive power and transformer tap ratio variations at both rectifier and inverter sides are shown in Fig. 13b and c.

Case 3 Minimization of total cost considering prohibited zones of thermal and wind-PV-PEV systems Minimizing the total cost while considering POZs as well as the cost models of wind, PV and PEV systems was studied in Case 3. The simulation result of SOS was 769.8551 $/h, which was better than those from the ABC, ICA, MSA, SFLA, GA and PSO methods, and the obtained results from those algorithms are given in Table 9. The convergence curves of the optimization algorithms, reactive power and transformer tap ratio variations at both rectifier and inverter sides for this case are shown in Fig. 14a–c, respectively. Figure 14 clearly shows that the SOS algorithm effectively converges to the optimal solution faster than the other methods, and the reactive power and transformer tap ratio variations are kept within the specified limits.

Case 4 Minimization of total cost emission and tax of thermal and wind-PV-PEV systems For Case 4, the optimization of the total cost with quadratic cost function and emission tax, as well as the cost models of the wind, PV and PEV systems used the objective function given in (26). The results obtained from the SOS, ABC, ICA, MSA, SFLA, GA and PSO optimization algorithms were 773.7498 $/h, 774.9863 $/h, 775.9863 $/h, 774.3481 $/h, 775.3144 $/h, 789.7627 $/h, and 774.1573 $/h, respectively. The objective value of the SOS algorithm was 1.2365 $/h, 2.2365 $/h, 0.5938 $/h, 1.5646 $/h, 16.0129 $/h, and 0.4075 $/h lower than those of the other

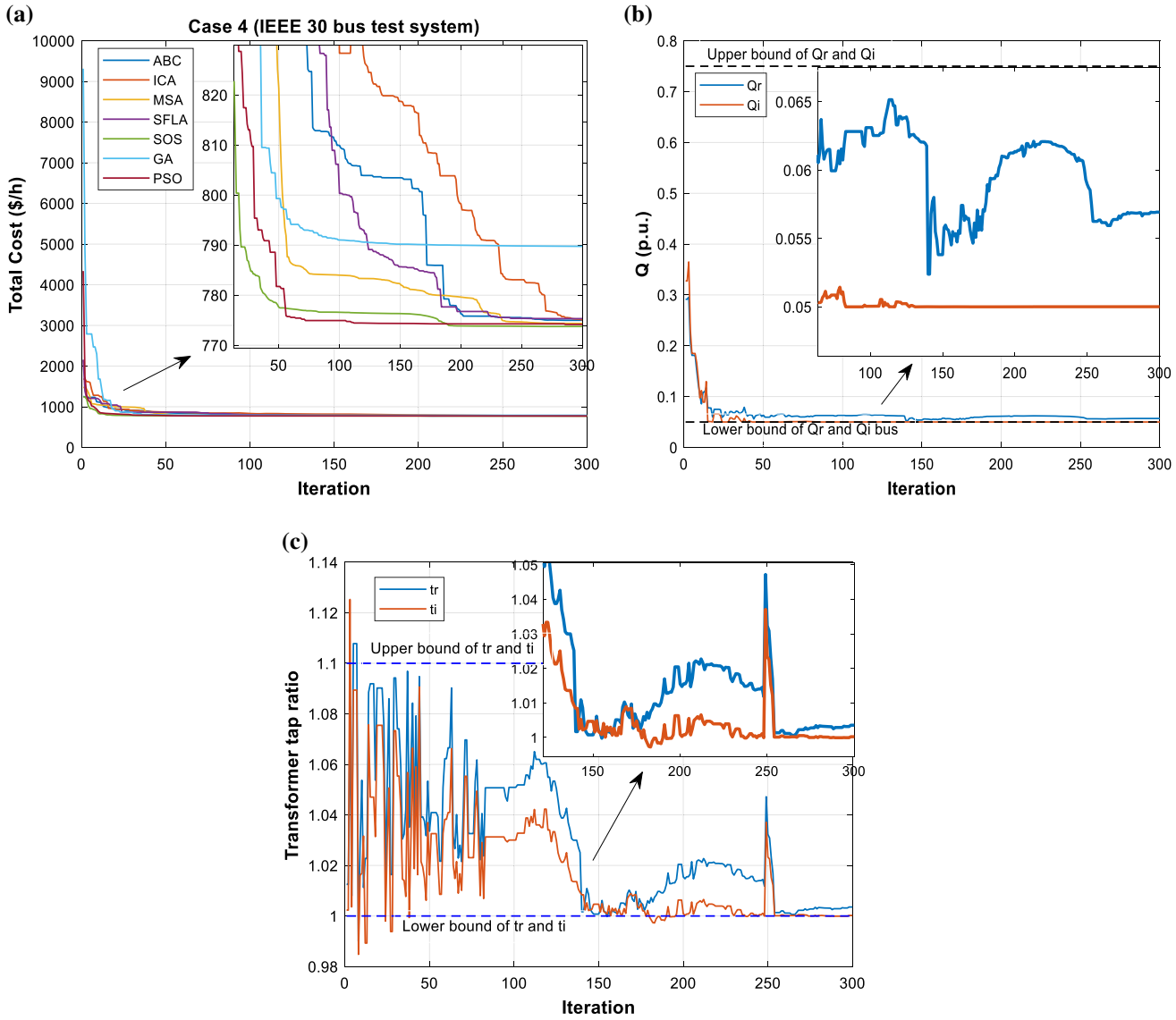


Fig. 15 Convergence curves of all algorithms, (**b**) reactive power (**c**) transformer tap ratio variations in rectifier and inverter sides (for Case4)

optimization algorithms. The convergence curves of the optimization algorithms, reactive power and transformer tap ratio variations at both rectifier and inverter sides for Case 4 are shown in Fig. 15a–c, respectively.

Case 5 Improvement voltage stability of test system The minimum *L*-index value for improvement of the voltage stability was studied for this case. The proposed objective function is given in (30). At the end of the optimization process, the minimum *L*-index values obtained by the SOS algorithm were better than those of the other optimization algorithms. That is, in Case 5, the result of SOS was 6.06395%, 3.46712%, 1.88284%, 3.68109%, 94.3795%, and 0.15801% lower than the simulation results of the ABC, ICA, MSA, SFLA, GA and PSO algorithms. Figure 16a and b shows the reactive power and transformer tap ratio variations at both rectifier and inverter sides, respectively.

Case 6 Minimization voltage deviation of test system Optimizing the voltage deviation of the system was studied for Case 6, and in (31) was considered as the objective function. In Case 6, the optimal simulation result obtained from SOS algorithm was 0.12445, which was 36.97570%, 14.76727%, 11.15157%, 17.93387%, 6.70215%, and 8.087149% lower than the results of the ABC, ICA, MSA, SFLA, GA and PSO algorithms, respectively. Changes of the reactive power and transformer tap ratio at both rectifier and inverter sides depending on iteration numbers are shown in Fig. 17a and b, respectively.

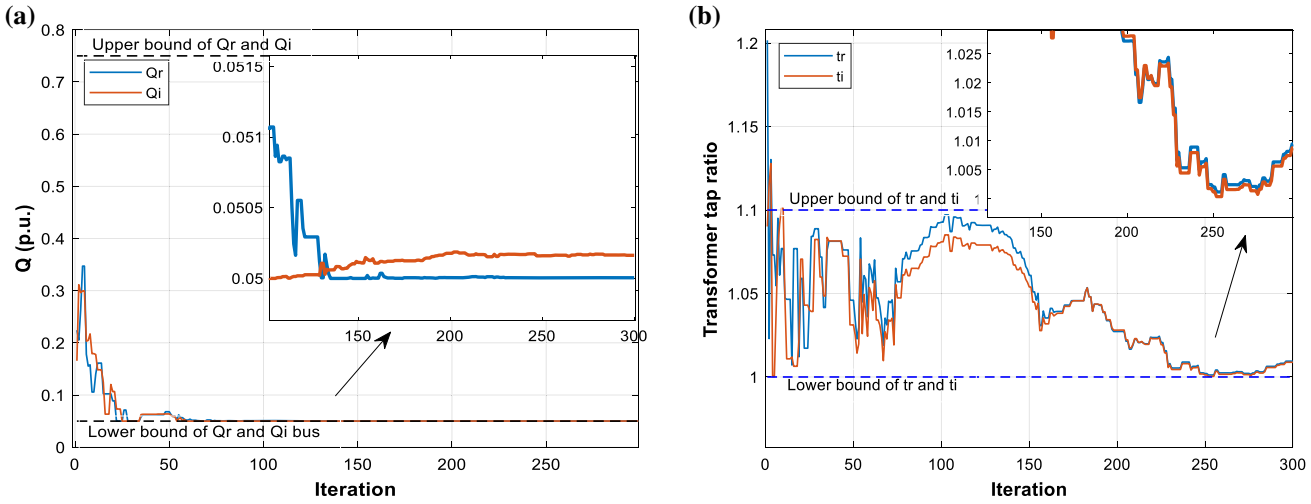


Fig. 16 **a** Reactive power **b** transformer tap ratio variations in rectifier and inverter sides (for Case 5)

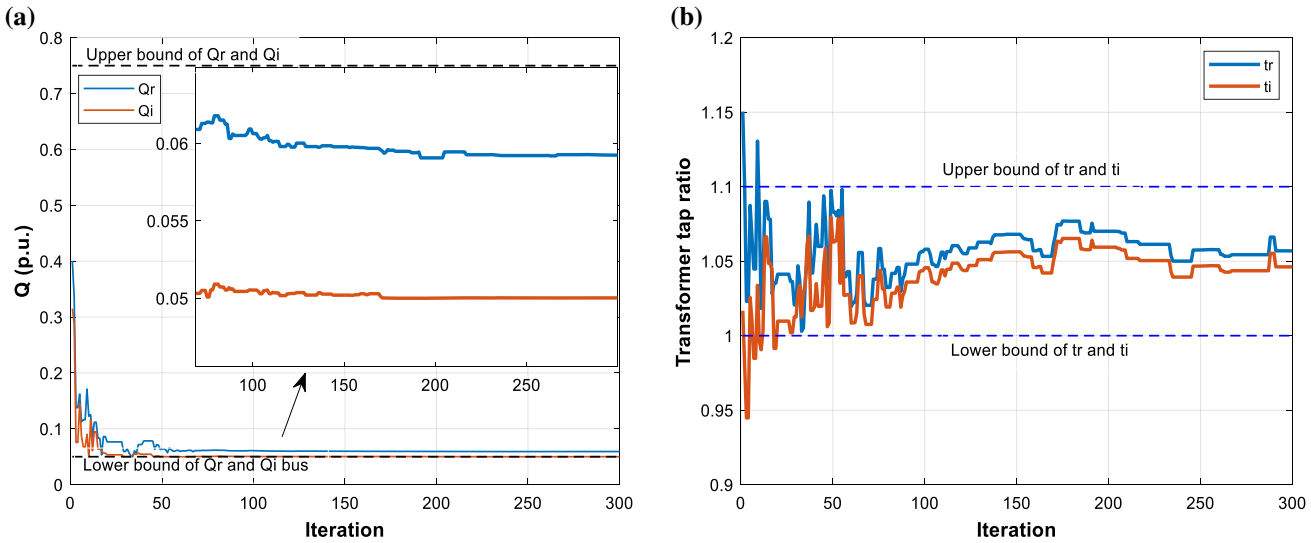


Fig. 17 **a** Reactive power **b** transformer tap ratio variations in rectifier and inverter sides (for Case 6)

Case 7 N−1 contingency conditions Different contingency conditions such as outages in the lines or the generating units might occur under continuous operating conditions in modern power systems. Thus, the power systems must have sufficient voltage stability under these conditions. In this case, to optimize both the total cost and enhancement of the voltage stability of the test system with two-terminal HVDCs, the objective function was considered as a single objective function and is given in (51).

$$f_{\text{obj}}(A_0, B_0) = F_{\text{obj}_1} + \left(\gamma_L \times F_{\text{obj}_5}\right) \tag{51}$$

In this study, we considered different contingency states, which included the outage of transmission lines between busses (15–23, 12–15, and 6–28). In the outage of the transmission lines between busses 15 and 23, the optimal simulation result of the SOS method was 784.9010, which was 4.4692, 1.306, 1.7884, 1.5893, 2.6329, and 0.7978 lower than the results of the ABC, ICA, MSA, SFLA, GA and PSO algorithms, respectively. The convergence curves of the optimal solution values of the optimization algorithms, reactive power and transformer tap ratio variations at both rectifier and inverter sides for Case 7.1 are shown in Fig. 18a–c, respectively.

Case 7.2 considered the contingency condition of an outage in the transmission lines between buses 12 and 15. The total cost values from the SOS, ABC, ICA, MSA, SFLA, GA and PSO methods were 786.4142, 788.5723, 787.7024, 788.1296, 787.9609, 787.417, and 787.73279, respectively.

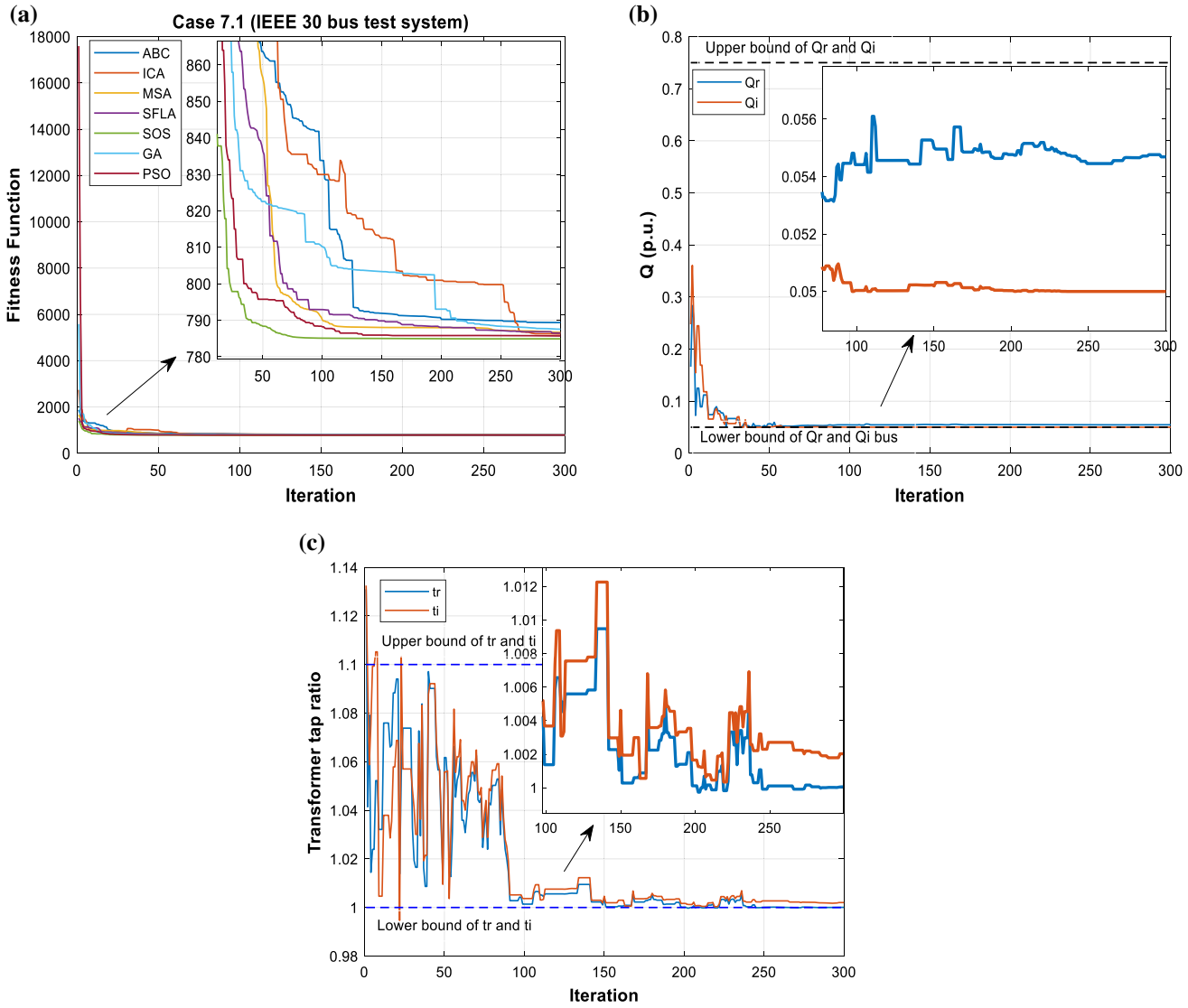


Fig. 18 Convergence curves of all algorithms, (**b**) reactive power (**c**) transformer tap ratio variations in rectifier and inverter sides (for Case7.1)

The minimum total cost value obtained by the SOS algorithm was better than the simulation results of the other optimization algorithms. Figure 19a–c shows the convergence curves of the optimal solution values of the optimization algorithms, change of the reactive power and the transformer tap ratio at both rectifier and inverter sides depending on iteration numbers, respectively.

An outage in the transmission lines between buses 6 and 28 was studied in Case 7.3. When the simulation results were examined, the best optimal result was obtained from the SOS algorithm, which was 785.3192. In other words, SOS algorithm was 1.7519, 1.6572, 2.005, 1.0941, 3.498, and 1.0074 lower compared with the simulation results of the other optimization algorithms.

The convergence curves of the optimal solution values of the optimization algorithms, change of the reactive power and the transformer tap ratio at both the rectifier and inverter sides depending on iteration numbers for Case 7.3 are shown in Fig. 20a–c, respectively. Figure 21a and b shows the voltage profile of all load buses for all cases, and these values are all within the specified upper and lower limitations.

5.2.2 Test system 2

In this part of the simulation, the studying conditions specified in Case 8, Case 9 and Case 10 were applied in IEEE 57-bus test system. The simulation results obtained from these Case studies are shown in Table 8. As can be

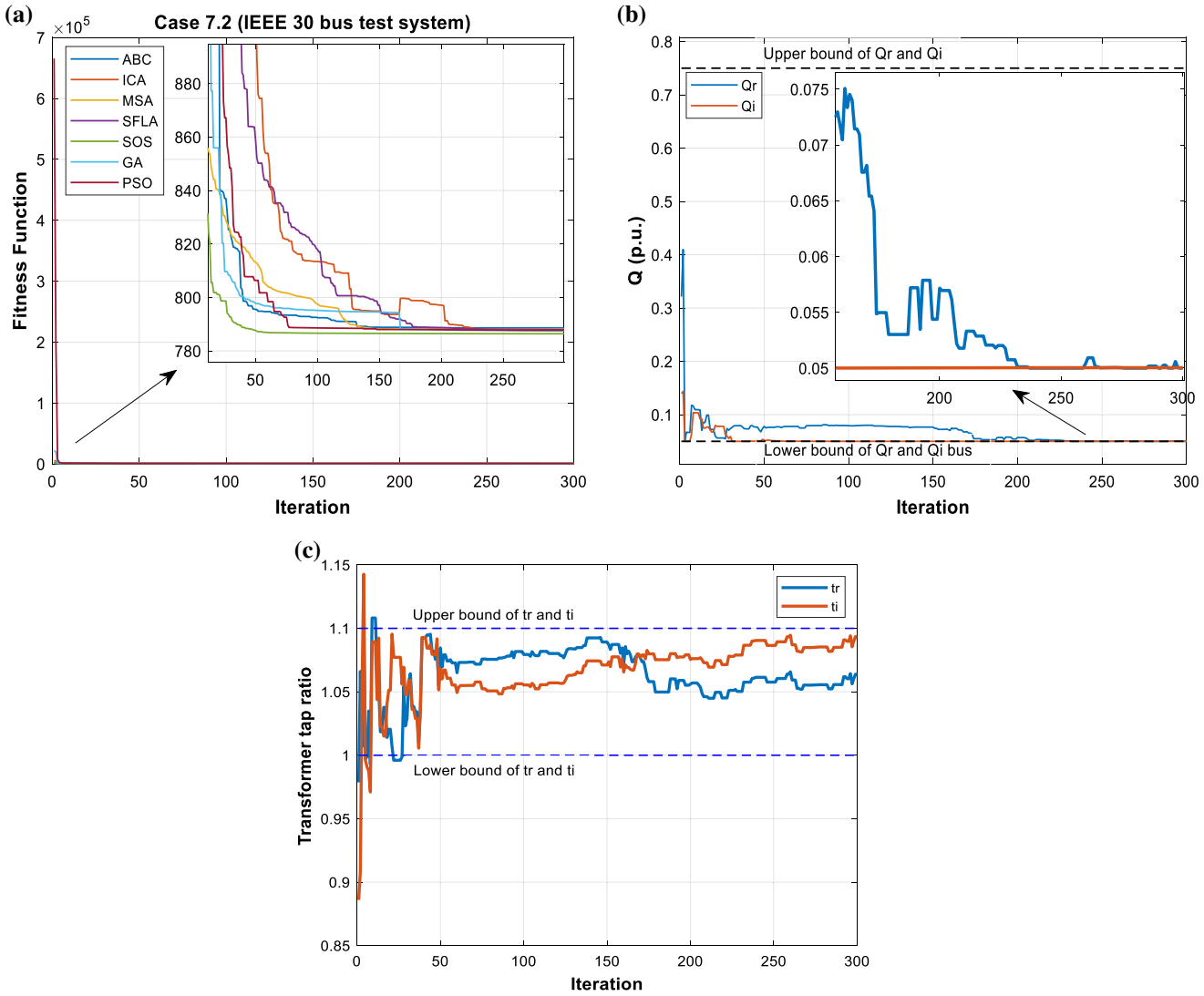


Fig. 19 Convergence curves of all algorithms, (**b**) reactive power (**c**) transformer tap ratio variations in rectifier and inverter sides (for Case7.2)

clearly seen from Table 8, according to the results obtained from the SOS algorithm, the control variables of the proposed problem are within the specified limit values. Furthermore, the simulation results obtained from all optimization algorithms for Case 8, Case 9 and Case 10 are given in Table 10 in detail. SOS, ABC, ICA, MSA, SFLA, GA and PSO algorithms are used to find the minimum value of the total cost considering the quadratic cost function of the thermal generators, the cost model of RESs and PEV systems in Case 8. Total cos value of the SOS is 30461.5781 $/h, which is 32.4612 $/h, 22.6133 $/h, 75.3092 $/h, 203.1576 $/h, 93.3473 $/h, and 56.5472 $/h, lower than the results from ABC, ICA, MSA, SFLA, GA and PSO methods, respectively.

The convergence curves of the fitness function value of all optimization algorithms for Case 8 are indicated in Fig. 22a. The proposed SOS algorithm converges to the optimal solution of the problem faster than the other algorithms. Figure 22b and c shows the reactive power and transformer tap ratio variations at both rectifier and inverter sides throughout the optimization period.

In case 9, minimizing of objective function value, the obtained results from the optimization algorithms are, respectively, 30463.6587 $/h, 30497.2068 $/h, 30530.3553 $/h, 30512.5751 $/h, 30839.2581 $/h, 30566.4826 $/h, and 30540.5587 $/h. In other words, the result of SOS algorithm is 0.11000%, 021845%, 0.16031%, 1.21792%, 0.33639%, and 0.25179% lower than the results of ABC, ICA, MSA, SFLA, GA and PSO algorithms, respectively.

The convergence curves to the optimal solution values of the optimization algorithms, change of the reactive power and the transformer tap ratio at both the rectifier and

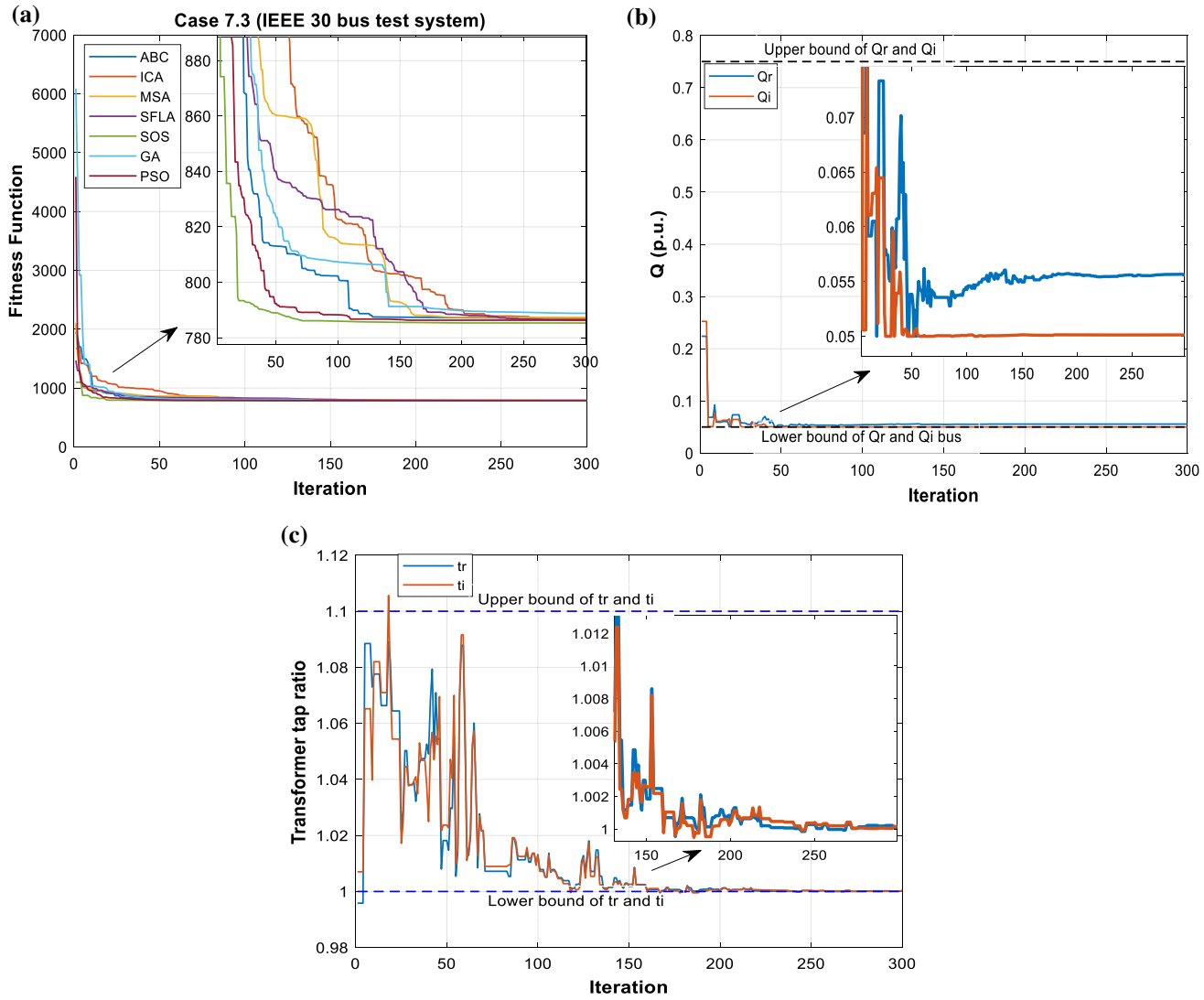


Fig. 20 Convergence curves of all algorithms, (**b**) reactive power (**c**) transformer tap ratio variations in rectifier and inverter sides (for Case7.3)

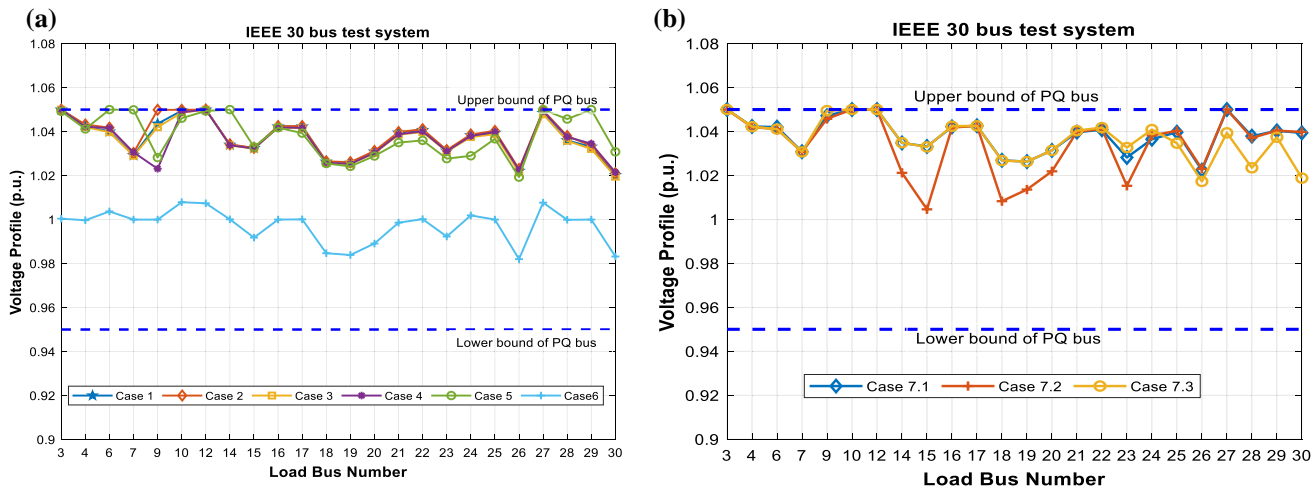


Fig. 21 Voltage profiles of load buses (**a**) for Case 1–6, (**b**) for Case 7.1–7.3

Table 8 Simulation results of the IEEE 57-bus test system

Parameters	Min.	Max.	Case 7	Case 8	Case 9	Parameters	Min.	Max.	Case 7	Case 8	Case 9
P_{PV+PEV} (MW)	− 16	80	60.4681	60.4713	60.5275	T_{80} (p.u.)	0.90	1.10	0.9331	0.9656	0.9698
P_{THG3} (MW)	40	140	41.6478	41.4051	41.6465	Q_{C18} (MVAr)	0	30	4.8277	18.5627	27.3024
P_{WS1} (MW)	0	150	149.9999	150.0000	149.9998	Q_{C25} (MVAr)	0	30	12.1913	13.4794	21.5149
P_{THG8} (MW)	100	550	423.3350	422.0996	426.2098	Q_{C53} (MVAr)	0	30	12.9181	12.5578	12.9894
P_{WS2} (MW)	0	120	119.9999	119.9997	119.9993	Pr (p.u)	0.10	1.50	1.3999	1.3992	1.3969
P_{THG12} (MW)	100	410	336.3365	334.6117	333.5928	Pi (p.u)	0.10	1.50	1.3966	1.3959	1.3936
V_1 (p.u.)	0.95	1.10	0.9870	1.0231	1.0179	Qr (p.u)	0.001	0.75	0.4708	0.5460	0.6670
V_2 (p.u.)	0.95	1.10	0.9809	1.0183	1.0143	Qi (p.u)	0.001	0.75	0.4217	0.4214	0.4206
V_3 (p.u.)	0.95	1.10	0.9799	1.0198	1.0196	i_d	0.05	1.00	1.0000	0.9995	0.9978
V_6 (p.u.)	0.95	1.10	0.9983	1.0403	1.0450	t_r	0.90	1.10	1.0830	1.0691	1.0958
V_8 (p.u.)	0.95	1.10	1.0099	1.0408	1.0483	t_i	0.90	1.10	1.0891	1.0532	1.0482
V_9 (p.u.)	0.95	1.10	0.9919	1.0256	1.0305	$\alpha(^\circ)$	5	30	5.8128	12.0951	18.7204
V_{12} (p.u.)	0.95	1.10	0.9772	1.0128	1.0138	$\gamma(^\circ)$	10	30	10.0011	10.0030	10.0053
T_{19} (p.u.)	0.90	1.10	0.9141	0.9002	1.0084	v_{dr}	1.00	1.40	1.4000	1.3999	1.4000
T_{20} (p.u.)	0.90	1.10	0.9207	1.0672	1.0127	v_{di}	1.00	1.40	1.3967	1.3965	1.3967
T_{31} (p.u.)	0.90	1.10	1.0236	1.0134	1.0103	P_{THG1} (MW)	0	576	133.3981	135.7873	132.6298
T_{35} (p.u.)	0.90	1.10	0.9025	0.9263	1.0472	Q_{THG1} (MVAr)	− 140	200	52.8642	45.6569	31.5403
T_{36} (p.u.)	0.90	1.10	1.0993	1.1000	1.0970	Q_{PV+PEV} (MVAr)	− 32	40	39.9556	39.9681	39.9895
T_{37} (p.u.)	0.90	1.10	1.0229	1.0164	1.0206	Q_{THG3} (MVAr)	− 10	60	36.8352	30.9134	21.6977
T_{41} (p.u.)	0.90	1.10	0.9347	0.9701	0.9796	Q_{WS1} (MVAr)	− 60	70	− 6.6355	2.9809	− 1.9699
T_{46} (p.u.)	0.90	1.10	0.9603	0.9567	0.9765	Q_{THG8} (MVAr)	− 140	200	101.4167	89.4819	107.9215
T_{54} (p.u.)	0.90	1.10	0.9105	0.9000	0.9001	Q_{WS2} (MVAr)	− 50	60	59.9983	59.9598	59.9724
T_{58} (p.u.)	0.90	1.10	0.9041	0.9426	0.9445	Q_{THG12} (MVAr)	− 150	155	55.9956	55.0165	54.8515
T_{59} (p.u.)	0.90	1.10	0.9018	0.9339	0.9366	Total cost ($/h)			**30461.5781**	**30463.6587**	**30429.374**
T_{65} (p.u.)	0.90	1.10	0.9120	0.9428	0.9465	Emission (t/h)			1.0985	1.0939	**1.1021**
T_{66} (p.u.)	0.90	1.10	0.9000	0.9136	0.9133	Carbon tax ($/h)			21.9704	21.8786	**22.0420**
T_{71} (p.u.)	0.90	1.10	0.9032	0.9425	0.9472	P_{loss} (MW)			14.0514	13.2411	13.4728
T_{73} (p.u.)	0.90	1.10	0.9973	0.9909	0.9817	VD (p.u.)			1.3273	1.3215	1.4296
T_{76} (p.u.)	0.90	1.10	0.9986	0.9696	0.9622	L-index			0.2867	0.2819	0.2852

inverter sides depending on iteration numbers for Case 9 are demonstrated in Fig. 23a–c, respectively.

The obtained fitness values from minimization of the total cost with quadratic cost function and emission tax, including the cost models of the wind, PV and PEV systems used the objective function are 30451.4160 $/h, 30498.4403 $/h, 30661.2765 $/h, 30541.0025 $/h, 30752.6626 $/h, 30586.3517 $/h, and 30533.0552 $/h in case 10, and according to these results, SOS algorithm has the best fitness value.

The convergence curves of the results obtained from the optimization algorithms to the optimal solution, change of the reactive power and the transformer tap ratio at both rectifier and inverter sides for Case 10 are shown in Fig. 24a–c, respectively. Figure 24d indicates the voltage profile of all load buses for all cases, and these values are all within the specified minimum and maximum constraints.

5.3 Statistical analysis

In this section, the statistical analysis of the optimization algorithms used in the solution of the proposed OPF problem was executed. All algorithms were run 30 times for each case to provide sufficient and strong evidence for statistical analysis. In addition, nonparametric Friedman and Wilcoxon tests are shown in this section to test the

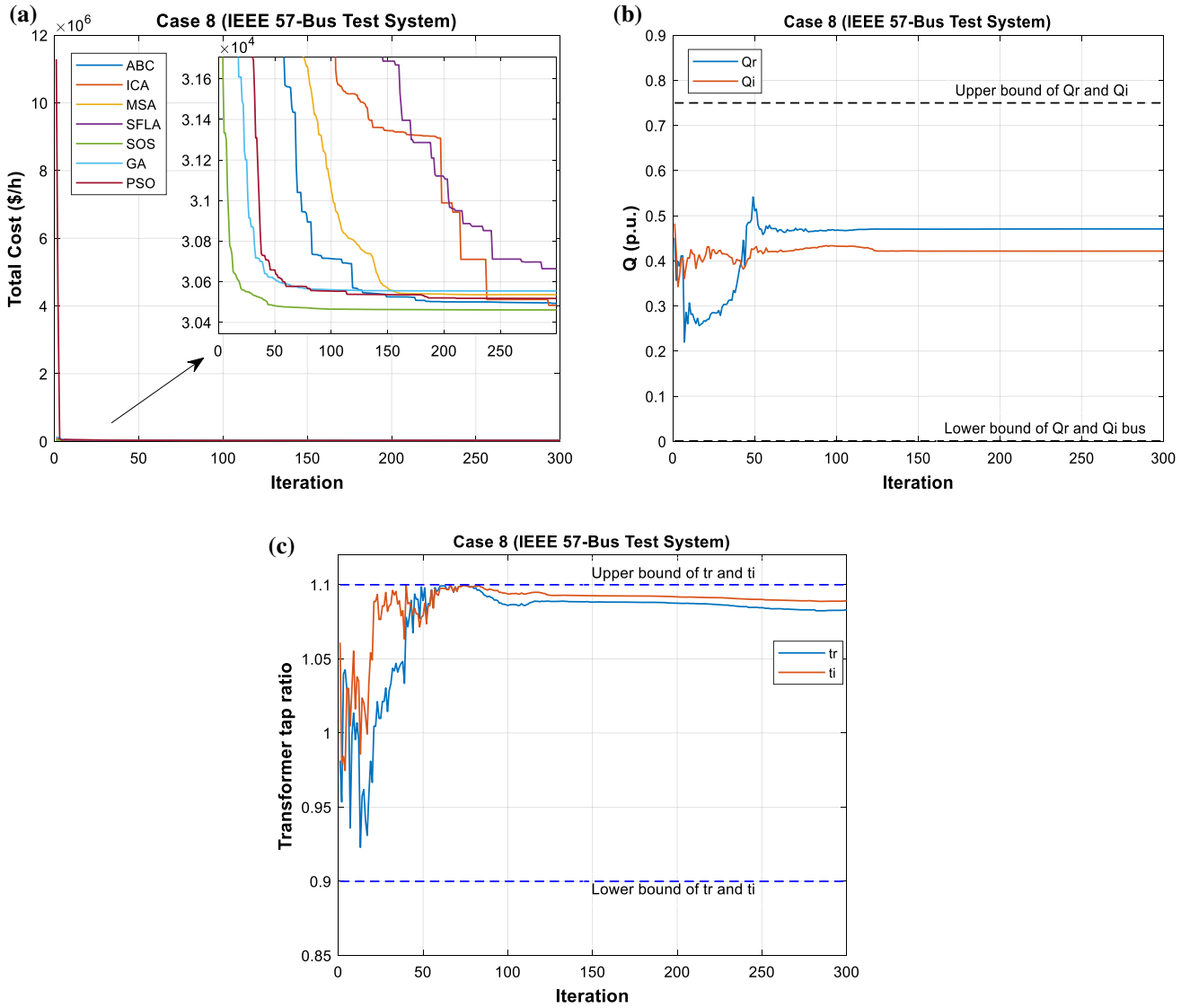


Fig. 22 Convergence curves of all algorithms, (**b**) reactive power (**c**) transformer tap ratio variations in rectifier and inverter sides (for Case 8)

statistical validity of the results obtained from the algorithms used in simulation studies (Carrasco et al. 2020).

Table 9 shows the minimum, mean, maximum, and standard deviation values of all the optimization algorithms used for the 30 runs in each simulation case and the computational times of all algorithms at the end of the optimization process. When the computational times of the SOS algorithm for all cases investigate, the SOS method is more successful on finding optimal solution of the problem than the other methods. That is to say, for Case 1, the computational time of the SOS algorithm is 2.9595%, 4.5941%, 2.5039%, 3.1104%, 7.2916%, and 6.7365% lower than the computational times of the other algorithms. It is clearly seen from Table 9 that the proposed algorithm is 2.9366%, 4.7041%, 3.0864%, 4.2682%, 6.9629%, and 5.5639% for case 2, 3.9938%, 4.5801%, 2.9503%, 3.6979%, 7.2700%, and 6.2968% for case 3, 4.3143%, 4.6082%, 3.1201%, 5.0458%, 8.4070%, and 6.4759% for case 4, 3.6753%, 3.3794%, 3.5276%, 2.6315%, 7.6358%, and 5.4135% for case 5, 4.0247%, 6.0606%, 5.3435%, 4.3209%, 9.2240%, and 6.2027% for case 6, 3.1722%, 3.3182%, 2.7735%, 4.4709%, 7.2359%, and 5.5964% for case 7.1, 3.4431%, 1.8264%, 2.4205%, 3.4431%, 7.0605%, and 5.4252% for case 7.2, 3.7707%, 3.0395%, 2.8919%, 3.9156%, 7.9365%, and 7.1324% for case 7.3 lower than the computational times of the ABC, ICA, MSA SFLA, GA and PSO algorithms, respectively. In other words, the computational times of the one iteration of the SOS algorithm are, respectively, 0.0692 s, 0.0697 s, 0.0694 s, 0.0690 s, 0.0698 s, 0.6888 s, 0.0712 s, 0.0716 s, and 0.0708 s for all cases. It is obviously seen that the SOS

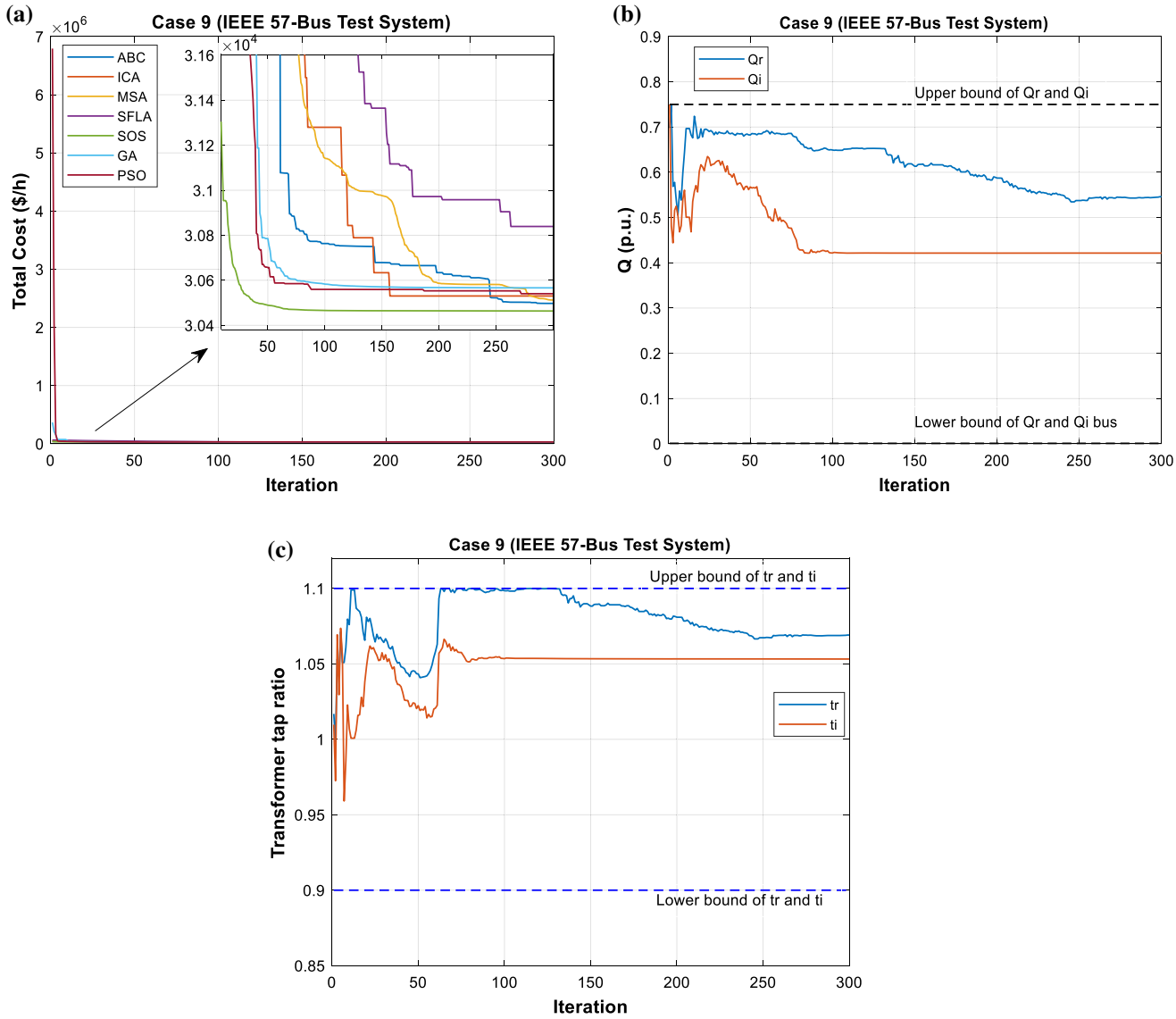


Fig. 23 Convergence curves of all algorithms, (**b**) reactive power (**c**) transformer tap ratio variations in rectifier and inverter sides (for Case 9)

algorithm is faster than the other algorithms according to the computational time of the one iteration.

According to the simulation studies performed under different operating conditions in the IEEE 57 bus test system, the minimum, mean, maximum and standard deviation values of the simulation results obtained as a result of 30 independent runs of the optimization algorithms used in the simulation studies are given in Table 10. When Table 10 is examined in detail, it is clear that the SOS algorithm is successful in all simulation situations, and has a better time compared to other algorithms in terms of computation time.

Table 11 is prepared in order to analyze the pairwise comparison results between the SOS algorithm and the other optimization algorithms in solving proposed OPF problem, and it is clear from Table 11 that the SOS algorithm shows superior performance compared to its competitors in all simulation studies. In other words, it can be said that the SOS algorithm prevails in each run compared to its competitors in 30 independent runs.

Table 12 shows the rankings of all algorithms according to the Friedman analysis method. While each row of Table 12 shows the performance of an algorithm, the Friedman ranking of the algorithms for each case is given in the columns of the table. In the last column, the mean rank of algorithms used for all simulation cases is listed. According to the results of Friedman analysis, it is clearly seen from Table 12 that the optimization algorithm that shows the best search performance among the algorithms used is the SOS algorithm.

According to the results obtained from 30 independent runs, the boxplots created in Fig. 25 are given for easy

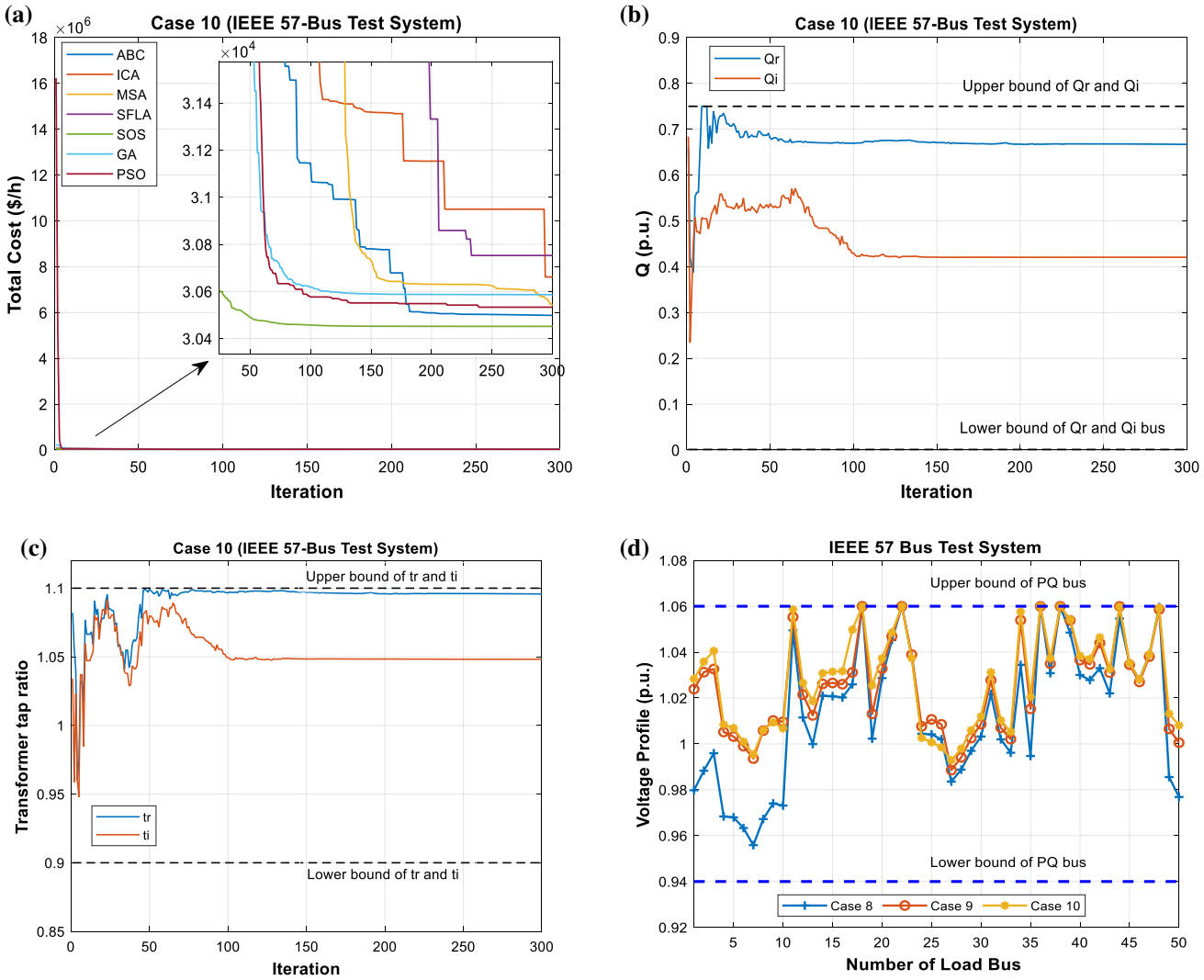


Fig. 24 Convergence curves of all algorithms, (**b**) reactive power (**c**) transformer tap ratio variations in rectifier and inverter sides (for Case 9), (**d**) Voltage profiles of load buses (for Case 8–10)

understanding and interpretation of the search performance of the optimization algorithms. When these graphs are examined in detail between Case 1 and Case 7.3 for IEEE 30-bus test system, it is seen that the minimum, maximum, mean and standard deviation values of the SOS and PSO algorithms are reasonable. However, it can be said that ABC, ICA, MSA, SFLA and GA algorithms are caught in local solution traps in most of study cases. It is clearly seen that especially the GA algorithm experiences premature convergence in all cases.

When the boxplot graphs for the IEEE 57 bus test system are examined, it is seen that the SFLA algorithm experiences early convergence and that other ABC, ICA, MSA, GA and PSO algorithms are caught in local solution traps.

6 Conclusion

The OPF problem is one of the most important issues addressed by power system researchers in the planning, operation and control of modern electrical power grids. Therefore, with the solution of this problem, it is aimed to ensure that modern power systems operate under the most suitable conditions. Simulation studies are carried out on different test systems under the diversified operating conditions, including various restrictions and limitations for this power system planning problem. The complexity of this problem has increased with the recent inclusion of renewable energy sources in modern power systems. With the increasing use of HVDC systems in power systems, the OPF problem has turned into an even more complex structure. In this study, in addition to traditional thermal generation units, wind, PV and PEV systems are also

Table 9 The obtained simulation results from all optimization algorithms for IEEE 30-bus test system

Methods	Case 1	Case 2	Case 3	Case 4	Case 5	Case 6	Case 7.1 (line outage (15–23))	Case 7.2 (line outage (12–15))	Case 7.3 (line outage (6–28))	
SOS	Min.	769.5928	798.8588	769.8551	773.7498	0.13601	0.12445	784.9010	786.4142	785.3192
	Mean.	769.6281	798.9400	769.8921	773.8296	0.1383	0.12896	784.9530	786.5344	785.4126
	Max.	769.7444	800.5908	769.9796	774.7271	0.14557	0.13444	785.0159	786.9892	785.5853
	Std.	0.0341	0.3123	0.03199	0.1882	0.00287	0.002442	0.0262	0.1108	0.06045
	Simulation time (s)	623	628	625	621	629	620	641	645	638
ABC	Min.	773.4497	801.2714	770.7626	774.9863	0.14479	0.19139	789.3702	788.5723	787.0117
	Mean.	780.4516	810.6725	811.6561	787.1968	0.35539	0.49256	798.1055	797.0708	794.9273
	Max.	799.7928	829.7790	869.7037	802.0090	0.62709	0.7848	811.2722	816.5843	808.3833
	Std.	6.7082	6.1371	28.1184	6.8329	0.13086	0.16344	5.9539	7.4226	5.2727
	Simulation time (s)	642	647	651	649	653	646	662	668	663
ICA	Min.	770.448	800.9689	771.9949	775.0523	0.140895	0.146012	786.207	787.7024	786.9764
	Mean.	784.0119	810.5947	787.9625	786.1262	5.28724	5.93946	795.0862	790.7534	800.5820
	Max.	800.7913	829.3908	806.7374	805.6676	22.0461	21.0918	813.6477	805.7996	816.7907
	Std.	7.5146	8.8594	8.5536	8.8990	6.42947	5.13557	7.1031	4.1764	8.8873
	Simulation time (s)	653	659	655	651	651	660	663	657	658
MSA	Min.	770.6341	800.093	770.8036	774.3481	0.13862	0.14007	786.6894	788.1296	787.3242
	Mean.	778.4452	808.0184	787.6961	785.3018	0.82624	1.24614	790.3733	793.8396	796.6137
	Max.	798.9423	832.0129	841.8255	808.1307	7.4615	18.7431	800.6311	821.0407	828.3598
	Std.	7.5327	8.6352	16.28127	10.0621	1.8963	3.981	3.2864	6.8742	10.5969
	Simulation time (s)	639	648	644	641	652	655	659	661	657
SFLA	Min.	771.6566	800.6337	771.5053	775.3144	0.141208	0.151646	786.4903	787.9609	786.4133
	Mean.	774.6622	806.4198	778.3977	778.7705	4.51455	4.41661	790.3568	790.1354	790.3483
	Max.	789.2341	822.5084	793.9391	789.3661	21.6783	38.0413	802.9600	795.6759	796.9345
	Std.	3.6505	6.1059	6.7456	3.2655	5.51259	7.42758	4.2016	1.8586	3.0789
	Simulation time (s)	643	656	649	654	646	648	671	668	664
GA	Min.	780.1213	811.9189	786.4577	789.7627	2.4199	0.13339	787.5339	787.417	788.8172
	Mean	810.9993	837.3178	809.8819	809.8982	28.4850	21.1976	809.5715	801.7137	812.9171
	Max.	844.9128	870.044	866.1560	842.5862	43.5353	40.8968	831.8696	834.5599	846.9134
	Std.	17.2175	15.6708	16.3436	11.3878	9.0246	10.6538	11.57467	12.90794	16.17724
	Simulation time (s)	672	675	674	678	681	683	691	694	693
PSO	Min.	770.5165	799.4172	770.4471	774.1573	0.13923	0.1354	785.6988	787.73279	786.3266
	Mean.	771.4128	800.0601	782.3494	775.0453	0.14252	0.14464	786.5138	789.3305	787.3543
	Max.	772.4835	801.5780	855.3082	776.1784	0.1451	0.16375	788.5339	795.7667	789.2546
	Std	0.5595	0.5229	16.2078	0.5636	0.0035	0.007254	0.724444	1.4838	0.690634
	Simulation time (s)	668	665	667	664	665	661	679	682	687

included in the OPF problem. To solve the complex OPF problem mentioned above, this article focuses on modeling an AC–DC OPF problem including conventional thermal, wind, PV and PEV energy systems and solving the proposed OPF problem using SOS and other heuristic algorithms in the literature.

Table 10 The obtained simulation results from all optimization algorithms for IEEE 57-bus test system

Methods		Case 8	Case 9	Case 10	Methods		Case 8	Case 9	Case 10
SOS	Min.	**30461.5781**	**30463.6587**	**30451.4160**	SFLA	Min	30664.7357	30839.2581	30752.6626
	Mean.	30,471.4005	30470.4472	30463.9715		Mean.	32353.9791	32352.5586	33269.4538
	Max.	30496.5483	30507.3955	30493.9616		Max.	37581.0876	37762.8179	38268.6783
	Std.	10.723412	10.532412	13.630955		Std.	1709.82623	1638.33192	2466.55024
	Simulation time (s)	722	725	723		Simulation time (s)	745	754	748
ABC	Min.	30494.0393	30497.2068	30498.4403	GA	Min.	30554.9524	30566.4826	30586.3517
	Mean.	30533.4217	30530.5074	30542.6862		Mean.	30581.0176	30593.1757	30611.7974
	Max.	30576.4419	30590.8033	30575.5147		Max.	30606.8802	30619.4262	30641.9175
	Std.	22.2281821	20.6266494	18.1491786		Std.	13.9045193	14.2439841	11.9367612
	Simulation time (s)	745	748	752		Simulation time (s)	787	792	793
ICA	Min.	30484.1914	30530.3553	30661.2765	PSO	Min.	30518.1253	30540.5587	30533.0552
	Mean.	31079.1200	31307.1304	31074.4494					
	Max.	31331.6025	31531.5630	31342.7010		Mean.	30556.1545	30574.4646	30563.5025
	Std.	220.998969	226.339791	185.16308					
	Simulation time (s)	756	762	760		Max.	30858.5067	30615.3084	30602.8680
MSA	Min.	30536.8873	30512.5751	30541.0025					
	Mean.	30632.9218	30656.7093	30690.4118		Std.	60.4374955	17.0071244	16.6329545
	Max.	30826.1275	30881.2368	31000.5407					
	Std.	75.3652806	80.6057139	115.172052		Simulation time (s)	779	782	787
	Simulation time (s)	741	744	743					

Table 11 Wilcoxon test comparison of results for all used algorithms

SOS versus + / = /−	Case1	Case 2	Case 3	Case 4	Case 5	Case 6	Case 7.1	Case 7.2	Case 7.3	Case 8	Case 9	Case 10
ABC	30/0/0	30/0/0	30/0/0	30/0/0	30/0/0	30/0/0	30/0/0	30/0/0	30/0/0	30/0/0	29/0/1	30/0/0
ICA	30/0/0	30/0/0	30/0/0	30/0/0	30/0/0	30/0/0	30/0/0	30/0/0	30/0/0	30/0/0	30/0/0	30/0/0
MSA	30/0/0	30/0/0	30/0/0	30/0/0	29/0/1	30/0/0	30/0/0	30/0/0	30/0/0	30/0/0	30/0/0	30/0/0
SFLA	30/0/0	30/0/0	30/0/0	30/0/0	29/0/1	30/0/0	30/0/0	30/0/0	30/0/0	30/0/0	30/0/0	30/0/0
GA	30/0/0	30/0/0	30/0/0	30/0/0	30/0/0	30/0/0	30/0/0	30/0/0	30/0/0	30/0/0	30/0/0	30/0/0
PSO	30/0/0	29/0/1	30/0/0	29/0/1	23/0/7	30/0/0	30/0/0	30/0/0	30/0/0	30/0/0	30/0/0	30/0/0

Table 12 Friedman test ranking of all algorithms

Algorithms	Case1	Case 2	Case 3	Case 4	Case 5	Case 6	Case 7.1	Case 7.2	Case 7.3	Case 8	Case 9	Case 10	Mean Rank
SOS	1.0000	1.0333	1.0000	1.0333	1.3000	1.0000	1.0000	1.0000	1.0000	1.0000	1.0333	1.0000	1.0333
PSO	2.1333	1.9667	3.3000	2.1333	1.9333	2.1000	2.1333	3.2667	2.3000	2.9333	3.2667	3.0667	2.5444
MSA	4.2333	4.2667	4.0667	4.5000	3.4333	3.5667	3.8000	4.7333	4.7333	4.6000	4.6000	4.5667	4.2583
ABC	4.8667	4.9333	5.6000	5.0000	4.5333	4.3667	5.6333	5.6667	5.0000	2.6333	2.1667	2.1000	4.3750
SFLA	3.7333	4.3000	3.3333	3.7000	4.8667	4.9333	4.0000	3.6333	3.4333	6.6667	6.6667	6.8333	4.6750
ICA	5.1333	4.7000	4.4000	4.8667	5.0333	5.4000	4.9000	3.6667	5.3333	6.0667	6.2000	6.1667	5.1556
GA	6.9000	6.8000	6.3000	6.7667	6.9000	6.6333	6.5333	6.0333	6.2000	4.1000	4.0667	4.2667	5.9583

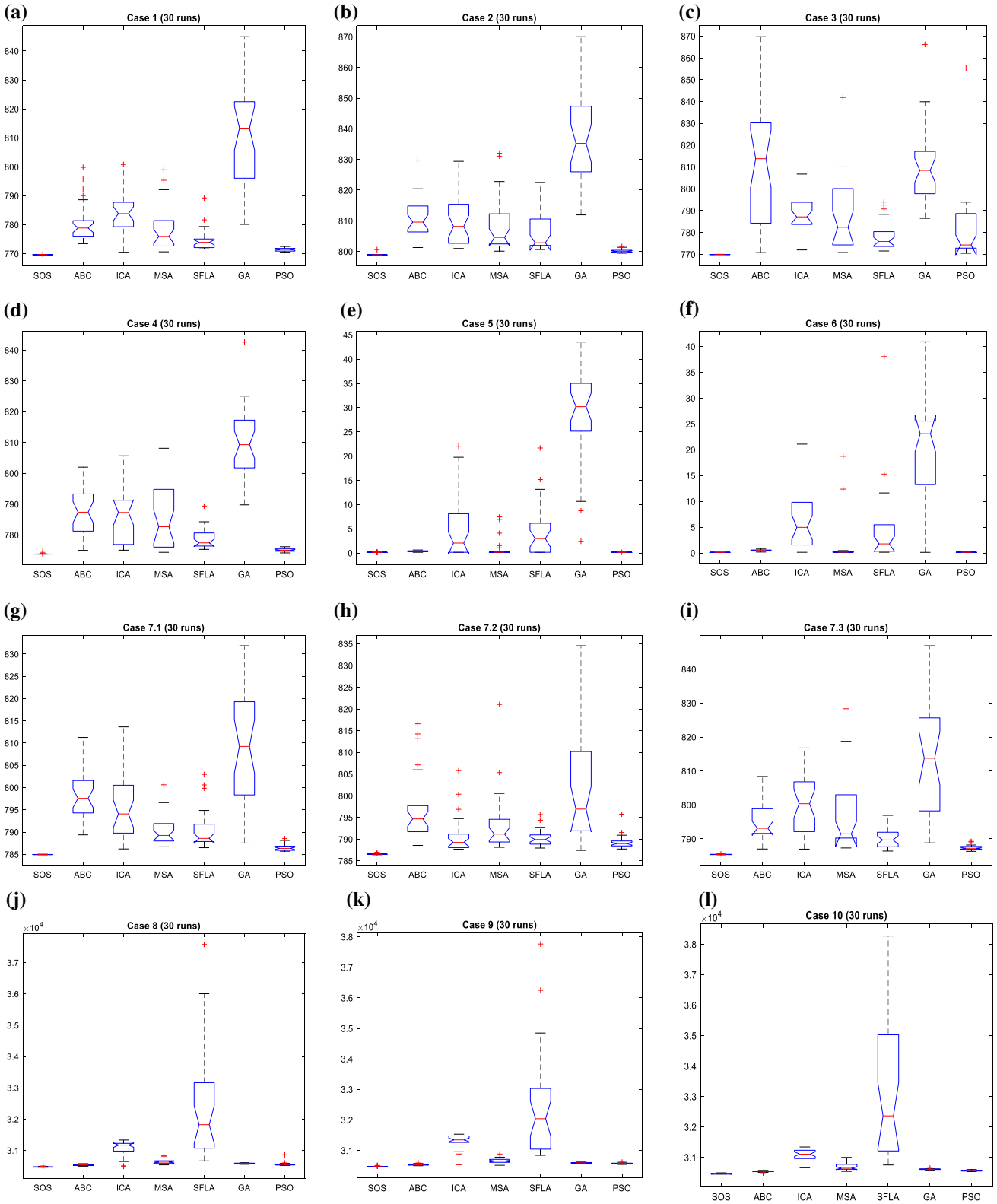


Fig. 25 Boxplot characteristics of all algorithms for 30 runs: **a** Case 1, **b** Case 2, **c** Case 3, **d** Case 4, **e** Case 5, **f** Case 6, **g** Case 7.1, **h** Case 7.2, **i** Case 7.3, **j** Case 8, **k** Case 9, **l** Case 10

The AC–DC OPF problem with RESs was tested on an IEEE 30-bus and 57-bus test systems via different cases involving voltage stability, voltage deviation, different thermal generating unit operating conditions and the selected$N-1$ contingency conditions. Additionally, the cost function models of the thermal generating units were considered under quadratic, valve point effect, and POZ operating conditions. The simulation results obtained from the SOS method for the different cases were compared to the results of ABC, ICA, MSA, SFLA, GA and PSO optimization algorithms. The comparison results demonstrated that the SOS provided a faster convergence speed to find a lower optimal solution value for fitness functions than the ABC, ICA, MSA, SFLA, GA and PSO methods. SOS algorithm has shown a powerful and effective performance as it converges to a better solution in minimizing the total cost and improving the voltage stability compared to other ABC, ICA, MSA, SFLA, GA and PSO methods. Furthermore, the SOS algorithm has the best computing time for all test cases according to the other heuristic methods. The SOS algorithm used in the solution of the intended problem is a heuristic algorithm that has been used in more than 700 studies in the literature and has been proven successful in solving various optimization problems.

Moreover, with the improved version of the SOS algorithm or using a constituted hybrid version of SOS with the other heuristics in the literature, future research may include: The application of the solution of the proposed problem approach in large power systems, using different constraint parameters, the dynamic OPF problem including renewable energy sources such as wind, PV, PEV, small hydro-power, tidal, and the solution of the dynamic multi-objective OPF problem with renewable energy can be investigated. In addition, it is suggested to model and investigate the solution of single and multi-objective problems involving multi terminal voltage-source converter (VSC) HVDC systems and renewable energy sources.

Acknowledgements Dr. Serhat DUMAN would like to thank the support provided by Scientific and Technological Research Council of Turkey (TUBITAK) BIDEB 2219 Postdoctoral Research Program under Application No. 1059B191700888.

Funding This study was not funded.

Declarations

Conflict of interest There is no conflict of interest between the authors to publish this manuscript.

Ethical approval This article does not contain any studies with human participants or animals performed by any of the authors.

References

Abdul-hamied DT, Shaheen AM, Salem WA, Gabr WI, El-Sehiemy RA (2020) Equilibrium optimizer based multi dimensions operation of hybrid AC/DC grids. Alex Eng J 59:4787–4803

Arevalo J, Santos F, Rivera S (2017) Application of analytical uncertainty costs of solar, wind and electric vehicles in optimal power dispatch. Ingeniería 22(3):324–346

Arevalo J, Santos F, Rivera S (2019) Uncertainty cost functions for solar photovoltaic generation, wind energy generation, and plug-in electric vehicles: mathematical expected value and verification by Monte Carlo simulation. Int J Power Energy Convers. https://doi.org/10.1504/IJPEC.2019.10018720,inpress

Atashpaz-Gargari E, Lucas C (2007) Imperialist competitive algorithm: an algorithm for optimization inspired by imperialistic competition. In: IEEE congress on evolutionary computation, pp 4661–4667

Attia AF, El Sehiemy RA, Hasanien HM (2018) Optimal power flow solution in power systems using a novel Sine-Cosine algorithm. Int J Electr Power Energy Syst 99:331–343

Ayan K, Kılıç U (2016) Optimal power flow of two-terminal HVDC systems using backtracking search algorithm. Int J Electr Power Energy Syst 78:326–335

Babu BS, Palaniswami S (2015) Teaching learning based algorithm for OPF with DC link placement problem. Int J Electr Power Energy Syst 73:773–781

Banerjee S, Dasgupta K, Chanda CK (2016) Short term hydro-wind-thermal scheduling based on particle swarm optimization technique. Int J Electr Power Energy Syst 81:275–288

Bansal JC, Joshi SK, Sharma H (2018) Modified global best artificial bee colony for constrained optimization problems. Comput Electr Eng 67:365–382

Biswas PP, Suganthan PN, Amaratunga GAJ (2017) Optimal power flow solutions incorporating stochastic wind and solar power. Energy Convers Manage 148:1194–1207

Biswas PP, Suganthan PN, Mallipeddi R, Amaratunga GAJ (2018a) Optimal power flow solutions using differential evolution algorithm integrated with effective constraint handling techniques. Eng Appl Artif Intell 68:81–100

Biswas PP, Suganthan PN, Qu BY, Amaratunga GAJ (2018b) Multiobjective economic-environmental power dispatch with stochastic wind-solar-small hydro power. Energy 150:1039–1057

Biswas PP, Suganthan PN, Mallipeddi R, Amaratunga GAJ (2019) Optimal reactive power dispatch with uncertainties in load demand and renewable energy sources adopting scenario-based approach. Appl Soft Comput J 75:616–632

Bouchekara HREH, Chaib AE, Abido MA (2018) Optimal power flow using GA with a new multi-parent crossover considering: prohibited zones, valve-point effect, multi-fuels and emission. Electr Eng 100(1):151–165

Cao J, Yan Z, Xu X, He G, Huang S (2016) Optimal power flow calculation in AC/DC hybrid power system based on adaptive simplified human learning optimization algorithm. J Mod Power Syst Clean Energy 4(4):690–701

Carrasco J, García S, Rueda MM, Das S, Herrera F (2020) Recent trends in the use of statistical tests for comparing swarm and evolutionary computing algorithms: Practical guidelines and a critical review. Swarm Evol Comput 54:100665

Chaib AE, Bouchekara HREH, Mehasni R, Abido MA (2016) Optimal power flow with emission and non-smooth cost functions using backtracking search optimization algorithm. Int J Electr Power Energy Syst 81:64–77

Chang YC, Lee TY, Chen CL, Jan RM (2014) Optimal power flow of a wind-thermal generation system. Int J Electr Power Energy Syst 55:312–320

Chen Y, Wei W, Liu F, Mei S (2016) Distributionally robust hydro-thermal-wind economic dispatch. Appl Energy 173:511–519

Cheng MY, Prayogo D (2014) Symbiotic organisms search: a new metaheuristic optimization algorithm. Comput Struct 139:98–112

Dubey HM, Pandit M, Panigrahi BK (2015) Hybrid flower pollination algorithm with time-varying fuzzy selection mechanism for wind integrated multi-objective dynamic economic dispatch. Renew Energy 83:188–202

Duman S (2017) Symbiotic organisms search algorithm for optimal power flow problem based on valve-point effect and prohibited zones. Neural Comput Appl 28(11):3571–3585

Duman S (2018) A modified moth swarm algorithm based on an arithmetic crossover for constrained optimization and optimal power flow problems. IEEE Access 6(1):45394–45416

El-Fergany AA, Hasanien HM (2018) Tree-seed algorithm for solving optimal power flow problem in large-scale power systems incorporating validations and comparisons. Appl Soft Comput 64:307–316

El-Fergany AA, Hasanien HM (2019) Salp swarm optimizer to solve optimal power flow comprising voltage stability analysis. Neural Comput Appl. https://doi.org/10.1007/s00521-019-04029-8

Eusuff M, Lansey K, Pasha F (2006) Shuffled frog-leaping algorithm: a memetic meta-heuristic for discrete optimization. Eng Optim 38(2):129–154

Ezugwu AE, Prayogo D (2019) Symbiotic organisms search algorithm: theory, recent advances and applications. Expert Syst Appl 119:184–209

Goldberg DE (1989) Genetic algorithms in search, optimization and machine learning. Addison-Wesley Longman Publishing Co., Inc., Boston

IEEE 57-bus test system data http://labs.ece.uw.edu/pstca/pf57/pg_tca57bus.htm

IEEE 30-bus test system data http://labs.ece.uw.edu/pstca/pf30/pg_tca30bus.htm

Jadhav HT, Roy R (2015) Stochastic optimal power flow incorporating offshore wind farm and electric vehicles. Int J Electr Power Energy Syst 69:173–187

Karaboga D, Basturk B (2007) A powerful and efficient algorithm for numerical function optimization: artificial bee colony (ABC) algorithm. J Glob Optim 39(3):459–471

Kathiravan R, Kumudini Devi RP (2017) Optimal power flow model incorporating wind, solar, and bundled solar-thermal power in the restructured Indian power system. Int J Green Energy 14(11):934–950

Kennedy J, Eberhart R (1995) Particle swarm optimization. In: International conference on neural network, pp 1942–1948

Kheshti M, Ding L, Ma S, Zhao B (2018) Double weighted particle swarm optimization to non-convex wind penetrated emission/economic dispatch and multiple fuel option systems. Renew Energy 125:1021–1037

Kılıç U, Ayan K (2014) Optimal power flow solution of two-terminal HVDC systems using genetic algorithm. Electr Eng 96(1):65–77

Kılıç U, Ayan K, Arifoglu U (2014) Optimizing reactive power flow of HVDC systems using genetic algorithm. Int J Electr Power Energy Syst 55:1–12

Kim S, Yokoyama A, Takaguchi Y, Takano T, Mori K, Izui Y (2020) Transient stability constrained optimal power flow in mixed AC/Multi-Terminal VSC HVDC system. IEEJ Trans Electr Electron Eng 15(10):1436–1447

Latorre HF, Ghandhari M (2011) Improvement of power system stability by using a VSC-HVdc. Int J Electr Power Energy Syst 33:332–339

Liang RH, Wang JC, Chen YT, Tseng WT (2015) An enhanced firefly algorithm to multi-objective optimal active/reactive power dispatch with uncertainties consideration. Int J Electr Power Energy Syst 64:1088–1097

MATPOWER http://www.pserc.cornell.edu/matpower/

Mohamed AAA, Mohamed YS, El-Gaafary AAM, Hemeida AM (2017) Optimal power flow using moth swarm algorithm. Electric Power Syst Res 142:190–206

Mohammadi F, Nazri GA, Saif M (2020) An improved mixed AC/DC power flow algorithm in hybrid AC/DC grids with MT-HVDC systems. Appl Sci 10(1):297

Mohseni-Bonab SM, Rabiee A, Mohammadi-Ivatloo B (2016) Voltage stability constrained multi-objective optimal reactive power dispatch under load and wind power uncertainties: a stochastic approach. Renew Energy 85:598–609

Morshed MJ, Hmida JB, Fekih A (2018) A probabilistic multi-objective approach for power flow optimization in hybrid wind-PV-PEV systems. Appl Energy 211:1136–1149

Naderi E, Kasmaei MP, Abdi H (2019) An efficient particle swarm optimization algorithm to solve optimal power flow problem integrated with FACTS devices. Appl Soft Comput J 80:243–262

Naderi E, Kasmaei MP, Cerna FV, Lehtonen M (2021) A novel hybrid self-adaptive heuristic algorithm to handle single- and multi-objective optimal power flow problems. Int J Electr Power Energy Syst 125:106492

Nguyen TT (2019) A high performance social spider optimization algorithm for optimal power flow solution with single objective optimization. Energy 171:218–240

Panda A, Tripathy M (2015) Security constrained optimal power flow solution of wind-thermal generation system using modified bacteria foraging algorithm. Energy 93:816–827

Panda A, Tripathy M, Barisal AK, Prakash T (2017) A modified bacteria foraging based optimal power flow framework for hydro-thermal-wind generation system in the presence of STATCOM. Energy 124:720–740

Prasad D, Mukherjee V (2016) A novel symbiotic organisms search algorithm for optimal power flow of power system with FACTS devices. Eng Sci Technol Int J 19:79–89

Prasad D, Mukherjee A, Mukherjee V (2017) Application of chaotic krill herd algorithm for optimal power flow with direct current link placement problem. Chaos Solitons Fractals 103:90–100

Qian K, Zhou C, Allan M, Yuan Y (2011) Modeling of load demand due to EV battery charging in distribution systems. IEEE Trans Power Syst 26(2):802–810

Reddy SS (2018) Optimal power flow using hybrid differential evolution and harmony search algorithm. Int J Mach Learn Cybern. https://doi.org/10.1007/s13042-018-0786-9

Reddy SS, Bijwe PR, Abhyankar AR (2015) Optimal posturing in day-ahead market clearing for uncertainties considering anticipated real-time adjustment costs. IEEE Syst J 9(1):177–190

Renedo J, Ibrahim AA, Kazemtabrizi B, García-Cerrada A, Rouco L, Zhao Q, García-González J (2019) A simplified algorithm to solve optimal power flows in hybrid VSC-based AC/DC systems. Int J Electr Power Energy Syst 110:781–794

Roy R, Jadhav HT (2015) Optimal power flow solution of power system incorporating stochastic wind power using Gbest guided artificial bee colony algorithm. Int J Electr Power Energy Syst 64:562–578

Saha A, Bhattacharya A, Chakraborty AK, Das P (2018) A powerful metaheuristic algorithm to solve static optimal power flow problems: symbiotic organisms search. Int J Electr Eng Inform 10(3):585–614

Saha A, Chakraborty AK, Das P (2019a) Quasi-reflection-based symbiotic organisms search algorithm for solving static optimal power flow problem. Sci Iran D 26(3):1664–1689

Saha A, Bhattacharya A, Das P, Chakraborty AK (2019b) A novel approach towards uncertainty modeling in multiobjective optimal power flow with renewable integration. Int Trans Electr Energy Syst 29(12):e12136

Saha A, Bhattacharya A, Das P, Chakraborty AK (2020) HSOS: a novel hybrid algorithm for solving the transient-stability constrained OPF problem. Soft Comput 24:7481–7510

Saric AT, Stankovic AM (2006) An application of interval analysis and optimization to electric energy markets. IEEE Trans Power Syst 21(2):515–523

Sayah S (2018) Modified differential evolution approach for practical optimal reactive power dispatch of hybrid AC–DC power systems. Appl Soft Comput J 73:591–606

Shaheen AM, El-Sehiemy RA, Elsayed AM, Elattar EE (2020) "Multi-objective manta ray foraging for efficient operation of hybrid AC/DC power grids with emission minimization", *IET Generation*. Transm Distrib. https://doi.org/10.1049/gtd2.12104

Shi L, Wang C, Yao L, Ni Y, Bazargan M (2012) Optimal power flow solution incorporating wind power. IEEE Syst J 6(2):233–241

Siavash M, Pfeifer C, Rahiminejad A, Vahidi B (2017) An application of grey wolf optimizer for optimal power flow of wind integrated power systems. In: 18th International scientific conference on electric power engineering (EPE), Kouty nad Desnou, Czech Republic, 17–19 May

Trivedi IN, Jangir P, Parmar SA, Jangir N (2018) Optimal power flow with voltage stability improvement and loss reduction in power system using moth-flame optimizer. Neural Comput Appl 30(6):1889–1904

Wang X, Chang J, Meng X, Wang Y (2018) Short-term hydro-thermal-wind-photovoltaic complementary operation of interconnected power systems. Appl Energy 229:945–962

Yalcin F, Arifoglu U (2014) Optimal reactive power flow solution in multiterminal AC–DC systems based on artificial bee colony algorithm. Turk J Electr Eng Comput Sci 22(5):1159–1176

Zeng B, Wei X, Zhao D, Singh C, Zhang J (2018) Hybrid probabilistic-possibilistic approach for capacity credit evaluation of demand response considering both exogenous and endogenous uncertainties. Appl Energy 229:186–200

Zeng B, Zhu X, Chen C, Hu Q, Zhao D, Liu J (2019) Unified probabilistic energy flow analysis for electricity-gas coupled systems with integrated demand response. IET Gener Transm Distrib 13(13):2697–2710

Zhao JH, Wen F, Dong ZY, Xue Y, Wong KP (2012) Optimal dispatch of electric vehicles and wind power using enhanced particle swarm optimization. IEEE Trans Industr Inf 8(4):889–899

Zhou J, Lu P, Li Y, Wang C, Yuan L, Mo L (2016) Short-term hydro-thermal-wind complementary scheduling considering uncertainty of wind power using an enhanced multi-objective bee colony optimization algorithm. Energy Convers Manage 123:116–129

Zimmerman RD, Murillo-Sanchez CE, Thomas RJ (2011) MATPOWER: steady-state operations, planning, and analysis tools for power systems research and education. IEEE Trans Power Syst 26(1):12–19

Publisher's Note Springer Nature remains neutral with regard to jurisdictional claims in published maps and institutional affiliations.